multi-Risk sciEnce for resilienT commUnities undeR a changiNg climate

Codice progetto MUR: **PE00000005** – CUP LEAD PARTNER: I33C22006910006

Deliverable title: Natural Hazards classification maps of point-like infrastructures of national relevance – Methodology Report

Deliverable ID: 6.3.2

Due date: February 2025

Submission date: February 2025

AUTHORS

Pierluigi Claps, Daniele Ganora, Paola Mazzoglio, Giulia Evangelista (POLITO), Salvatore Manfreda, Angelo Avino (UNINA); Monica Papini, Laura Longoni, Matteo Antelmi, Monica Corti (POLIMI); Antonello Barresi, David Castro Rodriguez (POLITO), Michele Torregrossa, Maria Castiglione (UNIPA); Paolo De Girolamo, Carolina Codato, Gioele Ruffini (UNIROMA1).

Approved by Paola Mazzoglio (WP leader)

1. Technical references

Project Acronym	RETURN
Project Title	multi-Risk sciEnce for resilienT commUnities undeR a changiNg climate
Project Coordinator	Domenico Calcaterra UNIVERSITA DEGLI STUDI DI NAPOLI FEDERICO II domcalca@unina.it
Project Duration	December 2022 – November 2025 (36 months)

Deliverable No.	DV3.2
Dissemination level*	PU
Work Package	WP3 - Dynamic mapping of natural and climatic hazards over the infrastructure systems
Task	T3.2 - Robust hazard mapping over point critical infrastructures (link with Spokes 1÷3)
Lead beneficiary	POLITO and POLIMI
Contributing beneficiary/ies	POLITO, UNINA, POLIMI, UNIPA, UNIROMA1

* PU = Public

PP = Restricted to other programme participants (including the Commission Services)

RE = Restricted to a group specified by the consortium (including the Commission Services)

CO = Confidential, only for members of the consortium (including the Commission Services)

Document history

Version	Date	Lead contributor	Description
0.1	04.02.2025	POLIMI and POLITO	First draft
0.2	11.12.2025		Critical review and proofreading
0.3	03.02.2025		Edits for approval
1.0	15.02.2025		Final version

2. Abstract

Similarly to Task 3.1, dynamic hazard selection criteria and maps are targeted, with robust and reliable methodologies, to produce hazard classification of individual, point-like critical infrastructures, such as dams, drinking water facilities and wastewater treatment plants. More specifically, the evaluation and mapping of natural hazard risks, particularly floods, sediments erosion, tsunamis and industrial asset vulnerabilities, across different sectors and geographical areas in Italy is taken in account. The main differences with respect to the approaches used in Task 3.1 attain the need to highlight the specific functions of each individual infrastructure, as well as the effects of hazards on the areas and users served.

This deliverable describes the products that were developed within the Task 3.2 of the Spoke TS2 to address these goals, which can be summarized in:

- the creation of a national-scale inventory of the Italian Large Dams complemented with more than 100 different catchment descriptors (Section 3.2.a);
- a national-scale assessment of the intrinsic flood attenuation potential of Italian Large Dams developed to identify the reservoirs best fitted for their flood mitigation efficiency (Section 3.2.a);
- assessment of the impact of dams on flood frequency curves (Section 3.2.a);
- development and application of sediment transport model (catchment-scale) to dam filling prediction and bottom openings interference in different geological contexts influencing sediment erosion and shallow water flow (Section 3.2.a);
- a place-based methodology for territorial vulnerability awareness including high-risk installations (e.g., drinking water and wastewater treatment plants), at various territorial scales (Section 3.2.b);
- development of a methodology aimed at calculating the areas and flooding speeds caused by tsunamis generated by earthquakes (Section 3.3.c).

In summary, all the activities aim to provide a comprehensive understanding of natural multi-hazards in key infrastructure sectors, enabling more informed risk management and mitigation strategies. The second part of the deliverable will instead focus on the application performed and the main results achieved.

3. Table of contents

List of Figures

3.2 Natural Hazards classification maps of point-like infrastructures of national relevance

3.2.a Enhanced hydrological hazard assessment on Large Dams

3.2.a.1 Flood Attenuation Potential of Italian Large Dams

3.2.a.1.1 Introduction

In the context of flood risk assessment and management, scientific contributions in the last decades have extensively investigated how the hydrological response of a basin can change significantly in the presence of artificial reservoirs (Balistrocchi et al., 2013; Manfreda et al., 2021; Volpi et al., 2018). However, an established methodological framework to assess the attenuation effects performed by dams has yet to be defined. More work still needs to be done to define the "natural", or rather "intrinsic", attenuation capacity of dams, referring to the "average" attenuation potential that depends only on the main structural characteristics of the reservoir and on the "main features" of the flood generated by the upstream basin. This means generalizing the observed situations as much as possible, a task that requires to use a conceptual framework.

Some efforts have been made to systematically assess the impact of reservoirs on flood peaks over large areas through synthetic indices. These indices aim to roughly quantity flood attenuation magnitude. Some of them are intended to be used as covariates in non-stationary frequency analyses, but they all provide information more in relative (comparative) terms than in absolute terms, as in many cases they lack dimensional consistency. Such approaches, however, can become particularly useful as quick tools for identifying the hydrological and hydraulic factors that most influence the mitigation effect, while accepting in some cases the oversimplification of the attenuation problem. Another popular approach involves stochastic rainfall simulations to derive hydrographs routed through reservoir systems, but this is typically case-specific and not easily scalable. At a national level, literature on the attenuation potential of dams is quite limited.

To fill these gaps, a comprehensive nationwide assessment of dam attenuation potential is provided, by identifying the most influential factors and ranking dams accordingly. The methodology adopted utilizes detailed infrastructure data, basin morphology, and state of the art rainfall extremes. To ensure consistency and scalability, a generalized framework is applied, including a simple hydrological scheme for design hydrographs and a "no gates management" approach with full hydraulic routing.

Simplified, yet rigorous and homogeneous assessment of the mitigation efficiency ranking can be used to prioritise the implementation of Dam Emergency Plans in Italy and to support similar initiatives worldwide.

3.2.a.1.2 Flood attenuation by reservoirs: definitions and assumptions

The flood peak attenuation by reservoirs is assessed by solving the continuity equation. For clarity and homogeneity of approach, the initial absolute water level in the reservoir is always considered equal to the absolute elevation of the spillway crest. For this reason, the variation of volume in time that is included in the continuity equation is intended as the change in storage volume above the elevation of the spillway crest. Based on this premise, which corresponds to the worst situation for flood attenuation, we consider the area of the lake to be constant with the lake surface elevation.

The attenuation coefficient, which varies between 0 and 1, is defined as the ratio of the outgoing and the incoming peak discharges, so that low values of the attenuation coefficient correspond to good attenuation capabilities. The attenuation coefficient is the index used to build a classification of the attenuation potential of reservoirs.

In our evaluations, only free-surface spillways are considered; furthermore, the outflow discharge dependence on the geometrical features of the spillway is assumed constant (i.e., no gates management is allowed). Furthermore, a Creager law is adopted for all spillways.

3.2.a.1.3 A Catalogue of "Great Dams" in Italy

One of the main motivations behind this assessment is to evaluate the attenuation potential of real dams, to obtain a priority ranking towards the development of Dam Emergency Plans, according to the Italian Directive 59/2004. To make this possible, a "Catalogue of Italian great Dams" (CID) has been compiled, that includes the characteristics of 528 large dams and of their upstream watersheds. The catalogue comprises the structures classified of national relevance, i.e. dams with a height of more than 15 metres or having a storage volume of more than one million cubic metres.

The surveillance of these dams is responsibility of the General Department of Dams (GDD) and Hydro-Electrical Infrastructures, part of the Italian Ministry of Infrastructures and Transports. About 75 % of the 528 large Italian dams are concrete dams and the remainder are earth dams. Most of them were built for hydroelectric and irrigation purposes.

The available structural parameters of the dams include, for instance, the elevation and the geometry of the reservoir spillway crests, as well as their lake areas. Geomorphological attributes of the basins upstream the dams were computed by processing the 30-m resolution NASA's Shuttle Radar Topography Mission (SRTM) digital elevation model (Farr et al., 2007) and considering only the area of the watersheds directly connected to the reservoirs, without reference to any indirectly connected basin.

It is worth adding that, to obtain realistic results, a systematic check of the values of the lake areas has been required. To this aim, the data provided by the GDD have been compared with surfaces extracted at the elevation of the spillway crests from a high-resolution DEM, i.e. the TINITALY/01 DEM (Tarquini et al., 2007) having a 10-m spatial resolution.

Before undertaking systematic analyses of the attenuation potential on all the dams of the CID catalogue, a pre-selection process has been conducted, intended to disregard dams for which a reasonable flood attenuation effect cannot be reached or is not meaningful. The following cases have been excluded:

- officially dismissed dams;
- dams already used as flood detention basins;
- dams where no attenuation volume is available or no unsupervised management is possible (this applies particularly on structures regulating large natural lakes);
- dams with very small lake areas in relation to the upstream watershed area (ratios lower than 1/150).

The resulting number of dams considered in the application is 265. The overall picture of the 265 watersheds considered presents mainly small, mountainous basins, as approximately 80% of them have an area of less than 100 Km^2 and more than 50% of them have an average elevation higher than 1000 metres above sea level.

3.2.a.1.4 Design flood hydrograph

The "standardized" incoming hydrographs are obtained with a 2-steps procedure: i) index-flood from the rational method (Mulvaney, 1851) is adopted as the incoming peak value; ii) the hydrograph shape is related to the flood volume in two ways: in a first instance, a rectangular incoming hydrograph is considered; in a second instance, an alternative formulation is used, in which a more complex dependence on the characteristics of the rainfall and of the basin morphology is considered. This formulation adopts a standardized symmetrical hydrograph, consistent with the flood reduction function, i.e., a curve representing, for a given duration, the maximum value of the average discharge computed on all the possible time windows of the same duration over the whole duration of the flood. A site-specific application of the (NERC, 1975) Flood Reduction Function is adopted.

The rational formula is used to simplify as much as possible the hydro-climatological factors controlling the design flood peak, including the key role of the rainfall parameters. This is particularly significant in Italy, where the knowledge of the spatial variability of rainfall extremes is supported by a richer data availability

as compared to floods. The subjectivity in the choice of the runoff coefficient, as well as the strong dependence of the results on the critical duration of the design rainfall, are dealt with here through a simple sensitivity analysis. As regards the runoff coefficient, no specific analysis of the surface runoff production is performed. Two possible values for the coefficient, i.e., 0.5 or 1 (referring respectively to low to medium permeability, and completely impermeable soil conditions) are considered. The lower value is widely referred to in technical literature (Rossi and Villani, 1994). Similarly, two formulations for the rainfall critical duration, i.e. for the basin time of concentration, are adopted. The first approach allows to estimate the time of concentration using the basin area only. In this case, the result will not be influenced by the basin and the river network morphology, which controls the kinematic features of the flood formation. The second approach is based on a formula that requires morphological watershed information. This sensitivity analysis is aimed at assessing how much a variation in the time of concentration, with all other parameters being equal, can affect the results in terms of reservoir attenuation capacity. Secondly, we aim to check how much the introduction of the morphological information content in the estimation of the time of concentration can affect the design flood peaks and, consequently, the ranking outcomes. The first formula used is the one by (Pilgrim and McDermott, 1981), while the second one is the Giandotti's (Giandotti, 1934).

To obtain design rainfall for each basin, areal-averaged Intensity-Duration-Frequency (IDF) curves are needed. This is quite a complex data requirement, as it involves the availability and the processing of a database of spatially distributed precipitation extremes. The rainfall data used to compute the areal IDF curves come from the Improved Italian – Rainfall Extreme Dataset (Mazzoglio et al., 2020), a systematic collection of annual maximum rainfall depths in 1, 3, 6, 12 and 24 consecutive hours, recorded over Italy by 5265 rain gauges between 1916 and 2019. The procedure for computing areal rainfall quantiles starts from the areal index rainfall intensity. Index rainfall curves have been first built at the rain gauge level. Then, at-station IDF parameters were spatially interpolated at a 250-meters resolution all over Italy, by using a ordinary kriging with the autoKrige function of the automap R package (Hiemstra, 2013). Finally, the spatially distributed values have been clipped within the basin boundaries and the areal averages have been computed.

With the same procedure, an areal average growth factor for every desired return period can be computed. For the purposes of this work, that essentially deal with a ranking approach to the flood attenuation potential of dams, it was considered to be reasonable to start with the index rainfall, that involved to assume a growth factor equal to 1 in every basin.

3.2.a.1.5 Rationale for a sensitivity analysis

For an overall rank assessment, each reservoir is assigned a number (rank), which identifies its position in the ordered vector of the attenuation coefficients (from the lowest to the highest values of the attenuation coefficient). To investigate the sensitivity of the ranking stability of the attenuation coefficients to the input parameters of the rational method, the incoming hydrograph to be routed by the reservoir is perturbed in 2 main ways. First, the design flood peak can be modified without varying the hydrograph time base. This effect can be obtained, for instance, by changing the runoff coefficient. The second type of modification adopted consists of changing the critical duration of the design rainfall, that directly modifies the hydrograph duration.

Type 1 distortion is introduced by using two different runoff coefficient values (C = 0.5 and C = 1) and two rainfall scenarios:

- scenario 1 uses a constant set of parameters to estimate the design rainfall, which represent the spatial average for all of Italy;
- scenario 2 uses site-specific parameters derived for each basin.

Type 2 distortion is introduced by varying the time of concentration, using three options:

- the time of concentration is calculated using Pilgrim and McDermott's formula;
- the time of concentration is calculated by amplifying 1.5 times the previous value;
- the time of concentration is calculated using Giandotti's formula.

By combining these variations, twelve different hydrographs are generated for each basin configuration, considering both rectangular and non-rectangular shapes. This results in a total of twenty-four hydrographs for analysis.

3.2.a.2 Flood Peak Attenuation of Large Dams and Detention basins

3.2.a.2.1 Introduction

During the last decades, the growing number of hydrological extremes has raised economic losses and risk perception worldwide. In this context, climate change and anthropic activities are probably accelerating the number of extremes. In fact, there has been a perceived global rise of flood hazards (Bertola et al., 2020) due to the catastrophic effects of several recent floods, resulting in damage and losses to the environment and communities (Di Baldassarre et al., 2010; Merz et al., 2021).

The increasing frequency and severity of floods have underscored the need for mitigation strategies. Detention basins can be effective tools for attenuating peak discharges. However, the proper design and management of a detention dam is extremely challenging due to its impact on the hydrological response of the basin. In addition, flood attenuation dynamics, caused by the presence of artificial reservoirs, are influenced by several hydrologic and hydraulic factors, such as flood wave shape and duration, as well as the storage capacity and geometric parameters of the basin, complicating its proper evaluation.

With this aim, new analytical-probabilistic approaches have been developed to interpret the functional relationships between inflows and expected outflows from dams. Several studies involved the use of theoretically derived probability distributions (Eagleson, 1972), which allowed hydrologists to move from a pure statistical to a more physically based approach. Theoretically derived probability distributions (TDD) have been widely adopted for flood maxima (Gioia et al., 2008), but also in many other contexts, representing a useful tool for deriving floods, droughts, water budget, scour, and hydropower production statistics in ungauged or gauged basins (Gioia et al., 2012; Iacobellis and Fiorentino, 2000). In this context, hydraulic and hydrological processes, such as flood peak lamination, can be driven by stochastic forcing. If the relationship between the variable and stochastic forcing is known, it is possible to analytically derive the probability distribution of the process. In particular, Manfreda et al. (2021) defined a theoretically derived probability distribution of the peak outflows from in-line detention basins, by assuming the incoming flood peaks to be randomly distributed and characterized by rectangular hydrographs of fixed duration. This framework was further explored by Albertini et al. (2022) to design a flood detection system in a river basin of southern Italy.

3.2.a.2.2 Modelling scheme and methodology

The main objective of the activities is to investigate the effect of flood control structures (dams) on downstream flood frequency curves by exploiting the approaches based on theoretically derived probability distributions (TDD).

Therefore, a new simplified analytical-probabilistic approach has been developed; specifically, a joint probability distribution of two theoretically derived probability distributions of i) the peak outflow from the dam and ii) the water level in the reservoir has been implemented. In particular, the proposed framework aims at extending the range of applications of the original formulation by Manfreda et al. (2021) by incorporating the initial state of water storage in the reservoir prior to each flood.

The conceptual scheme is represented by a reservoir dam (Figure 1).

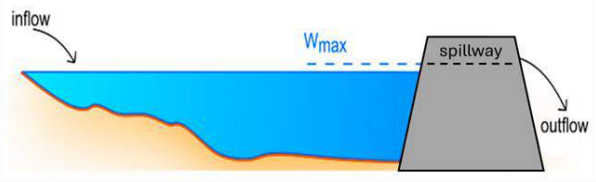

Figure 1: Sketch of a detention basin section with a basin capacity W_{max}, composed of a crest spillway of height h_s.

3.2.a.2.2.1 The theoretically derived probability distribution of the peak outflow from the dam

Let us first introduce the key equations controlling the dynamics of a system like the one under study. The first equation is represented by the stage-storage capacity curve; the function is generally represented by a power law:

$$W(h) = w_1 h^n \tag{3.2.1}$$

where:

- $W(h)$ [m^3] is the water storage of detention basin;
- w_1 [m^3] is the parameter of the stage-storage capacity curve;
- h [m] is the water level in the reservoir;
- n [–] is the exponent influenced by the shape of the control volume. The exponent ranges between 1 and 4.5, where 1 is associated with a prismatic geometry with vertical surrounding walls and 4.5 is associated with a more complex morphology closed by more gentle lateral slopes.

The outflow will be controlled by the amount of water accumulated in the system according to the continuity equation:

$$\frac{dW(t)}{dt} = Q_{in}(t) - Q_{out}(t) \tag{3.2.2}$$

where Q_{in} is the incoming flux and Q_{out} is the outflow from the reservoir.

The outflow can be computed using the traditional formulation of hydraulics based on the variation of the water level, h, in the reservoir, which can be derived from the stage-storage capacity curve (Eq. 3.2.1) and the continuity equation (Eq. 3.2.2). In particular, we assume that the outflow for the scheme displayed in Fig. 1 may vary according to two different discharge laws expressed as a function of the reservoir water level stage. The outflow can be described as follows:

$$\begin{aligned} Q_{out} &= 0 && \text{if } h \le h_s \\ Q_{out} &= \mu_s L_s \sqrt{2g}(h - h_s)^{\frac{3}{2}} && if\ h > h_s \end{aligned} \tag{3.2.3}$$

where h_s [m] is the height of the spillway crest, μ_s [-] is the coefficient of discharge of the spillway crest (suggested values range around 0.3-0.4 based on the geometry of the weir) and L_s [m] is the affected crest length.

As reported in Manfreda et al. (2021), the outflow is null as long as the reservoir is filled up to the regulation level, and thereafter, it is controlled by the crest spillway. In this last configuration, it is possible to use the linear reservoir concept for the water volume accumulated above the crest in order to estimate the peak outflow. When the volume below the spillway crest is totally filled, the crest spillway starts functioning. Therefore, the peak outflow, Q_{out}, assumes the following form:

$$Q_{out} = Q_{max}\left(1 - exp(-\frac{t - t_{filling}}{k})\right) \tag{3.2.4}$$

where Q_{max} is the peak flow, t [s] is the event duration, k [s] is the delay constant of the conceptual linear reservoir and $t_{filling} = \frac{W_{max}}{Q_{max}}$ is the activation time of the crest spillway (where W_{max} is the volume of water accumulated in the dam at the crest level, h_s).

The inverse function of the linear reservoir equation can be used to analytically compute the theoretically derived probability distribution of the peak outflow from the detention basin. The TDD can be derived once the relationship between the peak discharge, Q_{max}, incoming in the basin, and the peak outflow, Q_{out}, is inverted. The TDD equation is:

$$p(Q_{out}) = \left|\frac{dg^{-1}(Q_{out})}{dQ_{out}}\right| \cdot f_{Q_{out}}(g^{-1}(Q_{out})) \tag{3.2.5}$$

3.2.a.2.2.2 The theoretically derived probability distribution of the water level in the reservoir

The probability density function of the water level has been obtained by combining the stage-storage capacity curve (Eq. 3.2.1) and the probability density function of water volume in the reservoir, p_W.

In detail, the water balance equation for the water accumulated in the detention basin has been used to derive the pdf of water volume in the reservoir (p_W) by exploiting the approach of Manfreda and Fiorentino (2008). Specifically, the proposed water balance equation at the daily scale is:

$$\frac{dW(t)}{dt} = R - L \tag{3.2.6}$$

where:

- R [m^3] represents the daily runoff, with $R = \varphi A_b I$ (where φ is the coefficient of infiltration, A_b [m^2] is the area of the river basin and I [mm/day] is the mean daily rainfall);
- L [m^3] is the water losses (evaporation and water withdrawal) assumed to be constant;
- $W(t)$ [m^3] is the volume accumulated in the artificial reservoir (it is a function of the water level, $H(t)$, through the stage-storage capacity curve).

Specifically, by considering the mass conservation equation of the water volume in the reservoir, the rainfall forcing is considered as an additive noise (modelled by a sequence of instantaneous pulses that occur in a Poisson process), while the water losses (evaporation and water withdrawal) are assumed to be constant over time. Therefore, the pdf of water volume, p_W, has been derived following the approach of Rodriguez-Iturbe et al. (1999).

Ultimately, the TDD of the water level has been obtained by combining the stage-storage capacity curve (Eq. 3.2.1) and the probability density function of water volume (p_W). The expression of the TDD is:

$$p(H) = \left|\frac{df^{-1}(H)}{dH}\right| \cdot p_W(f^{-1}(H)) \tag{3.2.7}$$

At the end, the two obtained TDD (water level in the reservoir and peaks outflow from the dam) have been combined with a joint probability distribution.

3.2.a.3 Sediment transport model for dam filling prediction

3.2.a.3.1 Introduction

A quantitative estimation of the sediment volume will be provided for different geological contexts affecting erosion and discharge (liquid discharge and sediment yield). A literature review was carried out to identify the most widely used and effective direct methods to evaluate sediment volumes as a function of dam trapping capacity, and indirect methods to evaluate the sediment supply from the basin to the reservoir. Among the indirect methods, basin-scale models able to estimate sediment sources were used, such as the SMART-SED model (Gatti et al., 2023), developed in recent years at the Politecnico di Milano. The basin-scale models can estimate the maximum volume of sediments that can be deposited in a reservoir as a function of various factors, such as geologic and topographic variations in the basin, rainfall patterns, soil erodibility. A calibration analysis of the main physical parameters of the model was performed and different scenarios were developed with the aim to predict the dam filling in chosen case studies.

3.2.a.3.2 Direct and indirect approaches to evaluate sediment volumes

The volume of sediments filling a dam can be evaluated by means of different techniques: direct or indirect. In general, for the submerged part, surveys can be carried out either by bathymetric surveys (coupled or not with GPS system) distributed or concentrated in sections, whereas for the part emerged topographic or photogrammetric surveys can be carried out. Among the direct methods, the main approaches are:

1. Direct survey of the sediment thickness, conducted at variable points in number and location, includes the following methods:
   a) Techniques with full reservoir, such as the sub-bottom profiler. The accuracy of the survey depends on the difference in texture between the sedimented material and the original reservoir bottom. It is also influenced by the water head and the morphology of the reservoir bottom. Another technique is the direct survey of sediment thickness through bottom borings, performed by appropriately equipped vessel, with sampling of the material or surveying its mechanical characteristics in situ (e.g., penetrometric tests).
   b) Techniques with empty reservoir, such as direct survey of sediment thickness by drilling the reservoir bed, with material sampling, in situ mechanical characterization (penetrometric tests) or performing geophysical or geoelectric surveys. Again, the accuracy depends on the density and extent of the surveys carried out, in addition to the difference in consistency of the sedimented material from the original background material.
   c) The Brune method (Brune, 1953), which is an approach depending on the dam "trapping" capacity. It requires the input and output of the sediments on the basis of solid transport measurements upstream and downstream of the dam. Moreover, it requires the evaluation of the yearly average flow rate through the reservoir.

2. Indirect survey of the sediment thickness, conducted at variable points in number and location, includes the following methods:
   d) Techniques with full reservoir, such as boat bathymetry on predefined sections. In this case, the survey accuracy depends on the number and distance of sections, the density of points surveyed in each section, as well as the morphology of the reservoir bottom and the water depth. Another method involves the use of differential GPS equipment synchronized with a single- or multibeam echosounder, installed on a boat and connected to fixed points on land. The accuracy of the survey depends on the accuracy of the instrumentation, density of surveyed points, bottom morphology and water depth. Another approach is measuring the derived flow rate at different elevations over a predetermined time frame, detecting the corresponding changes in water level and natural inflow rate. In this case, the accuracy is independent of the ground morphology and the water draught.
   e) Techniques with empty reservoir, such as ground topographic-type techniques. In this case, the accuracy of the survey can vary widely, depending on the class of instruments adopted, the configuration of the survey network, the density of points surveyed, and the morphology of the reservoir bottom. Another method is with terrestrial or aerial photogrammetric techniques; in this case the survey accuracy is variable depending on the equipment used, the scale of the photos and their adaptation to the areas to be surveyed, the density of the points returned, and the morphology of the bottom;
   f) USLE/RUSLE method (Amore et al., 2004): evaluates the solid transport to the dam depending on 6 main factors, influenced by various parameters linked to the erosion process in the basin upstream of the dam. The product of factors allows to estimate the yearly average soil loss (ton/ha) through the formula: $E = R \cdot K \cdot L \cdot S \cdot C \cdot P$, where R is the rainfall erosivity factor, K the soil erodibility factor, L and S the factors dependent on basin topography, C the factor depending on the effect of crops, cultivation techniques or vegetation, P the factor effect of conservation practices.
   g) WEPP (Flanagan and Livingston, 1995) is a continuous simulation model that is able to predict spatial and temporal distributions of net soil loss and deposition for a wide range of time periods and spatial scales. The Hillslope version computes erosion along a single slope profile, while the Watershed version can be used to assess soil loss at the catchment scale. In this latter case, the watershed is idealised with multiple hillslopes, channels and impoundments. The model is composed of several components, taking into account climate, hydrology and water balance, plant growth with residue decomposition and agricultural practices, soil composition and consolidation.

In particular, with regard to weather, WEPP can read climate data from two different input files: CLIGEN (Nicks et al., 1995) or BCDG, i.e. Breakpoint Climate Data Generator (Gete et al., 1999).

h) Geographical information system (GIS) based model named TopRunDF (Maris et al., 2019) used to predict the sedimentation area and the sediment deposition height in the sedimentation cone. The TopRunDF 2.0 model is a two-dimensional simulation tool used for the spread of load-bearing materials and for the prediction of the quantity of sediment deposition on the sedimentation cone. Based on the topography of the torrential fan, the model combines a simple flow routing algorithm with the area-volume relation. It is developed with the programming language Visual Basic 6.0 and performs as an integrated executable program using objects of the geographic information system ArcGIS. The input data of TopRunDF are the volume of sediments, the mobility coefficient, a dimensionless parameter reflecting the flow properties throughout the depositional procedure, the deposition's starting point and the digital terrain model of the watershed. The output results forecast the deposition zones and the height of sediments in these zones. The main advantage of this model lies in the fact that it does not require demanding and time-consuming data, while the accuracy of the results remains notable.

i) The Erosion Potential Method (EPM) from Gavrilovic (Kostadinov et al., 2018): this method was developed for the estimation of the sediment production and has been used widely in the Balkan countries since the late 1960s for erosion and torrent-related problems. According to this specific method, the soil erosion is expressed with the following equation:

$$W = T \cdot h \cdot \pi \cdot (\sqrt{Z^3}) \tag{3.2.8}$$

where W is the average annual production of sediments (m^3/year), T is the temperature coefficient (-), h is the mean annual precipitation (mm), Z is the erosion coefficient (-), and F is the area of the catchment (km^2). The temperature coefficient T is given by the following formula:

$$T = \sqrt{(\frac{t_0}{10} + 0{,}1)} \tag{3.2.9}$$

where t_0 is the mean annual temperature (°C) of the basin (Auddino et al., 2015). The mean annual precipitation h was calculated with the use of GIS with the same aforementioned method for the calculation of the R factor of the USLE method. The erosion coefficient Z has been evaluated as:

$$Z = \mathrm{x} \cdot \mathrm{y} \cdot (\varphi + \sqrt{J}) \tag{3.2.10}$$

where x is the soil erodibility coefficient (-) expressing the geological medium resistance reduction during erosion, y is the soil protection coefficient (-) depending on the petrological composition of the watershed, φ is the coefficient of type and extent of erosion (-), and J is the average slope of the surface of the catchment (%) calculated with the use of GIS.

j) SWAT model (Douglas-Mankin et al., 2010): the Soil and Water Assessment Tool is a physically-based hydrologic model developed by the USDA-ARS to predict the effects that land management has on runoff and sediment production in big and morphologically complex basins and heterogeneous in terms of soil and land use (Arnold et al., 1998). In the SWAT model, the basin is divided into sub-basins, which are further subdivided into homogeneous Hydrologic Response Units (HRUs) in terms of soil and land use characteristics. HRUs are spatially undefined virtual units computed by treating soil and land use information, as statistical distributions and transforming distributed spatial information (soil and land use maps) into non-spatial information. The efficient use of nonspatial datasets (Srinivasan et al., 2000) and the minimal computational costs of simulations, in which spatially distinct homogeneous areas in terms of land use are treated as single units (Neitsch et al, 2002), are the advantages offered by HRUs. It is therefore implied that there is no interaction between different HRUs: runoff volume, sediment production, nutrient and pesticide amounts, are evaluated in the single HRU and then summed for the single subbasin.

The resulting quantities leaving the subbasins reach the outlet section of the basin through the hydrographic network taking into account the possible presence of backwaters and/or reservoirs in the basin.

k) SMART-SED (Sustainable MAnagement of sediment transpoRT in responSE to climate change conDitions) model was developed by Politecnico di Milano (Brambilla et al., 2018; Gatti et al., 2023) and yields catchment wide outcomes of hydrological processes on an adaptive time step. In particular, the main advantages of this new tool are the automatic identification of the drainage network, the statistical downscaling of the soil input maps (Gatti et al., 2021), the few and commonly open input data required and the automatic handling of a wide range of transients. This model proved its reliability after its application case studies with different geological settings (Corti et al., 2023).

3.2.a.3.3 SMART-SED approach: methodology

The SMART-SED model was initially created during the SMART-SED (Sustainable Management of sediment transpoRT in reposnSE to climate change conditions) project under Fondazione Cariplo funding, while the last update version was carried during the PNRR project. The SMART-SED model is a physically-based sediment erosion and transport model, able to simulate hydrological processes at catchment scale. It operates on an adaptive time step, which gives greater accuracy to results and reduces computational costs. The model can recognize automatically both storage and erosion areas at the same time, as well as water discharge, by applying the fundamental conservation laws of mass and momentum (Bonaventura et al., 2021; Brambilla et al., 2020; Gatti et al., 2023). SMART-SED is classified as a distributed model, where the area under analysis is subdivided into square pixels that contains different layers of processes interacting among each other under specific topographic and meteorological forces, as sketched in Figure 2. At surface level, the model simulates atmospheric processes, rainfall and snow, based on temperature, drainage under different slope conditions, and sediment yield. On the other hand, the ground level is defined as a "soil zone" and it is internally divided into a gravitational layer, needed for the infiltration and evapotranspiration processes, and an erodible layer that is configured as the sediment source (Bonaventura et al., 2021; Brambilla et al., 2020; Gatti et al., 2023).

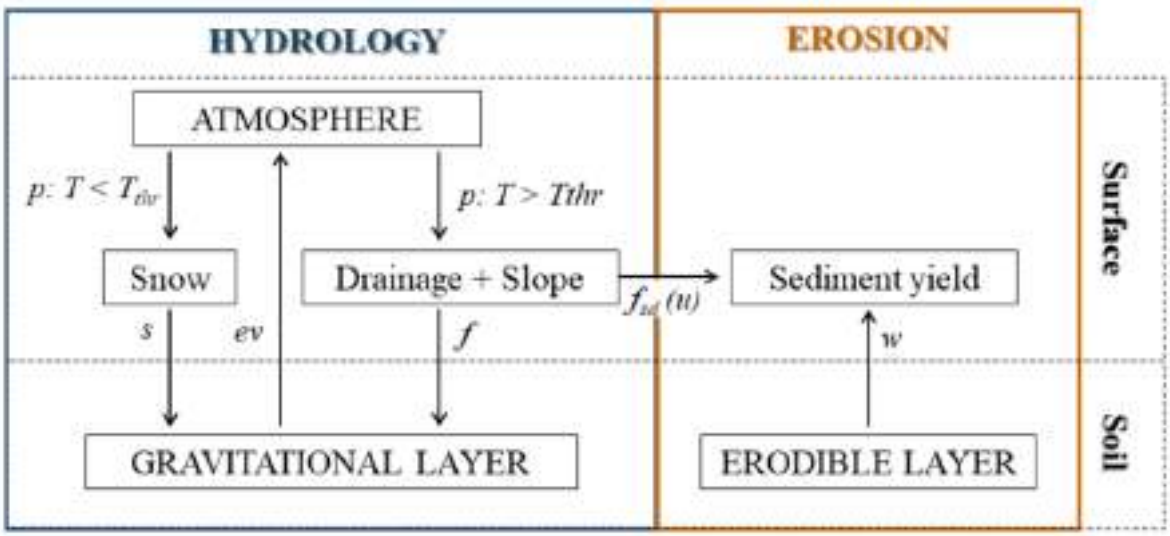

Figure 2: Conceptual scheme of SMART-SED model modified after Brambilla et al. (2020). The arrows represent the horizontal and vertical fluxes among adjacent pixels and different layers; *p* is precipitation, *T* is temperature, *s* is snow melt, *ev* is evapotranspiration, *f* is infiltration, *w* is sediment erosion, $f_{sd}(u)$ is flux.

The model is also equipped with a geostatistical pre-processor, described in Gatti et al. (2021), which downscales granulometric soil composition maps to a finer resolution. Each component of the model structure is summarized in the following. For further details, the full description of the mathematics behind SMART-SED is in Bonaventura et al. (2021) and in Gatti et al. (2023).

- *Atmosphere*: it is considered as an infinite capacity reservoir, whose outflow is the precipitation, *p*, characterized by its own intensity, duration, and distribution. Precipitation can be interpreted either as rain or snow depending on the surface temperature. The snow melting is regulated according to the Degree-days approach (Day, 2006) and the relative temperature threshold is set as 2°C. Atmosphere can receive water from the soil (gravitational layer) through evapotranspiration, *ev*, which is implemented according to the Hargreaves equation (Hargreaves and Allen, 2003).
- *Drainage zone*: it is the part of the surface in which shallow water is collected from runoff. In correspondence of this layer, the full de Saint-Venant equations are used to model water flow, to account also for water courses and larger water bodies such as lakes. This zone is variable in time: cells are activated when the water level reaches a critical threshold value. In these ways, it is not necessary to static pre-definition of the drainage network by the users, as in other models. Drainage, u, is controlled by slope. The roughness coefficient is determined with a formulation suitable for steep slopes and mountain streams that has been discussed in the works from Rickenmann (1994, 2001). The water discharge is then derived from the water mass flux, which is the product between the maximum water depth and the water velocity in the respective cell, times the cell size.
- *Gravitational layer*: this is a water storage layer at soil level, where motion is mainly by gravity. The loss of water towards the upper layer occurs through evapotranspiration. On the other hand, the water supply comes from snow melt, s, and infiltration, f, which follows the SCS curve number method (Rallison, 1980).
- *Erodible layer*: it represents the layer of erodible material, and it is used as a source term, *w*, for the computation of the sediment yield. The sediment source term, *w*, is defined according to the Erosion Potential Method from (Gavrilovic, 1988) as the rate of sediment production due to erosive processes after precipitation.
- *Sediment yield*: it is actually computed by the model as a flux and it is expressed as a function of the surface runoff velocity, of the sediment height and of the local terrain slope, following the approach of Zhang et al. (2009). Data required as input is often open data, such as the digital elevation model of the catchment, the land cover, the granulometric soil composition and logical data (temperature and precipitation). The latter are inserted together with the coordinates of the relative rainfall stations, so the model applies the Inverse Distance Weighted method for the spatial interpolation on the entire catchment area. If necessary, it is also possible to consider a spatially uniform precipitation. The input data required for the simulations described in this paper were downloaded from "Geoportale Regione Lombardia" website as regards the 5x5 m DEM (Regione Lombardia, 2023), from "Arpa Lombardia" website as regards the meteorological data (Regione Lombardia, 2021), from the CORINE Land Cover database as regards the land cover data (Copernicus, 2023) and from SoilGrids database for the granulometric soil composition (ISRIC, 2021).

The input data for the correct execution of SMART-SED model are constituted by raster maps: catchment area, land cover (e.g., Corine Land Cover), Digital Elevation Model (DEM), and soil granulometry (e.g., SoilGrids). In addition to this, the model requires weather data (precipitation and temperature from gauges near the study area) provided as text files for the event to be simulated. The input data can mostly be retrieved from open-source databases. For the numerical calibration of the model, data related to sediment erosion or sediment transport (for example estimated through bathymetries) and water discharge (or water table measures through hydrometers) are also required.

In summary the main peculiarities of the SMART-SED model are:

- Few simple inputs, which are often open data.
- Statistical downscaling of granulometric composition soil maps (SoilGrids).
- Automatic determination of the drainage zones.
- Automatic handling of a wide range of transients.
- Adaptive time step

3.2.b Place-based methodology for territorial vulnerability awareness (Using Geographical Information Systems - GIS)

3.2.b.1 Vulnerability of areas of concern around industrial assets (Seveso Industries) using a multi-hazard and multi-scale approach.

3.2.b.1.1 Contextualization of industrial assets within the European framework on the control of major risks installations and the resilience of critical entities.

The European Commission acknowledged in a report on the implementation of the EU strategy on adaptation to climate change that if the current trends in climate change keep going, the critical infrastructure in Europe would experience a huge increase in annual damage by the end of the century (see Figure 3), with the industry being among the sectors with higher vulnerability to suffering losses (European Commission, 2018).

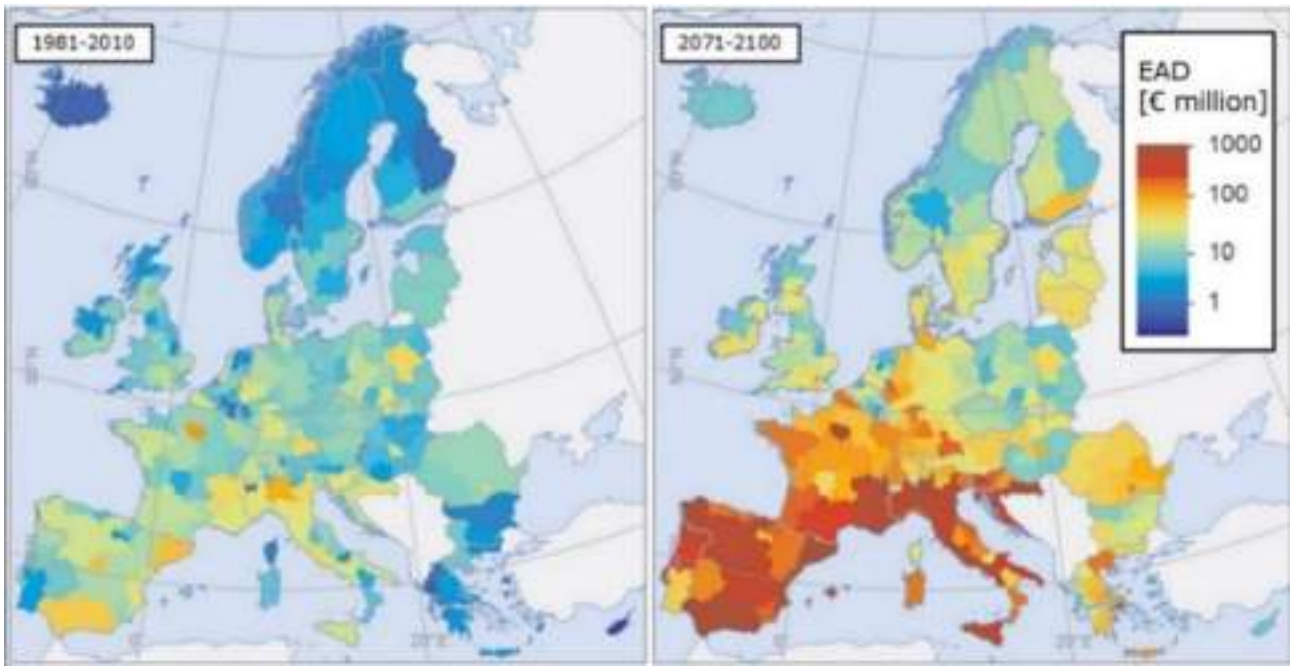

Figure 3: Expected annual damage to critical infrastructures in European regions, due to climate change, by the end of the century (million EUR). Source: European Commission (2018).

Considering this, the European Commission has recently released Directive (EU) 2002/2557 (European Union Parliament, 2022) to strengthen the resilience of critical entities. To address the issue of vulnerability, this directive orders that Member States identify critical entities and evaluate the risks associated with them establishing a national strategy by January 2026, to ensure resilience. Based on this evaluation, critical entities should adopt the relevant organizational and technological steps to guarantee their resilience, including steps to mitigate vulnerabilities. On the other hand, the directive does not include any explicit instructions or methodology about how vulnerabilities should be handled. Moreover, the document stipulates in article 5, point 2, that when Member States conduct risk assessments, they must consider the pertinent risk assessments that have been conducted in compliance with the requirements of the applicable sector-specific Union legislation, such as 2012/18/EU – Seveso III (European Union Parliament, 2012) sectors belonging to Major Hazard Industries (MHIs) are regarded as critical entities. In addition, is explicit that they should take into consideration all relevant natural and man-made hazards that might result in an incident. Therefore, it is foreseen in the future, the necessity to develop a coherent link between the current transposition of directives 2012/18/EU (on the control of major-accident hazards involving dangerous substances) within the realities of each Member State, and the forthcoming transposition of (EU) 2022/2557 (on the resilience of critical entities) mainstreaming the international strategies for achieving sustainability, prevention disaster, and loss prevention (Castro Rodriguez, 2024).

3.2.b.1.2 Addressing the concept of vulnerability/resilience within the current Italian transposition of the European framework.

As mentioned before, there is an explicit necessity to integrate risk evaluations between the current Seveso III directive (2012/18/EU) and the future (EU) 2022/2557 transposed directive. This integration aims to strengthen the resilience of critical industrial entities that are at risk from multiple hazards in their surrounding territory, including steps to identify their vulnerabilities. However, neither explicit instructions nor methodologies are included in the referred legal framework about how vulnerabilities should be handled, or the resilience be enhanced. From this gap, the following research question arises: How effectively does the legal framework for Seveso III address the resilience/vulnerability concepts for Industrial Critical Infrastructures (ICIs) within multi-hazard contexts?

Even if resilience emerges as a central topic in the debate on hazards affecting socio-ecological and technological systems (SETSs), this approach is a broadly employed concept with different definitions and views depending on the context and the characteristics of interest (Hosseini et al., 2016). A broad concept was chosen that defines resilience as "the capacity of the system –and all its socio-ecological, technical, and infrastructural components– to preserve or rapidly return to basic functionalities, so responding to turbulence and/or shocks, the adaptation to climate change, and the transforming of subset components which limit the present and/or the future evolution capacity" (Davoudi et al., 2013). In the context of critical infrastructure systems, the resilience is analyzed into three phases attending the disruption profile (Jain et al., 2017). It implies actions before, during, or after a disturbance.

Specifically, before the disturbance, it involves promptly identifying vulnerabilities within the system to prevent potential disruptions. Vulnerability, in the context of climate change, refers to the system elements predisposition (susceptibility) to be damaged punctuality by hazardous events or continuous pressures over time (Intergovernmental Panel on Climate Change, 2023). Identifying vulnerabilities is often seen as the counterpart to building resilience. Therefore, this phase is the cornerstone for enhancing resilience by focusing on anticipation and monitoring pillars (Hollnagel et al., 2006) during the normal performance of the system.

To figure out the answer to the previously stated research question, the Italian industrial context was selected as a representative case study among European Member States. The last public report on the implementation and efficient functioning of the Seveso III Directive has registered 11,776 establishments distributed in the different European Member States (see Figure 4), with a proportion of 43% and 57% for upper-tier establishments (UTE) and lower-tier establishments (LTE) respectively (European Commission, 2021).

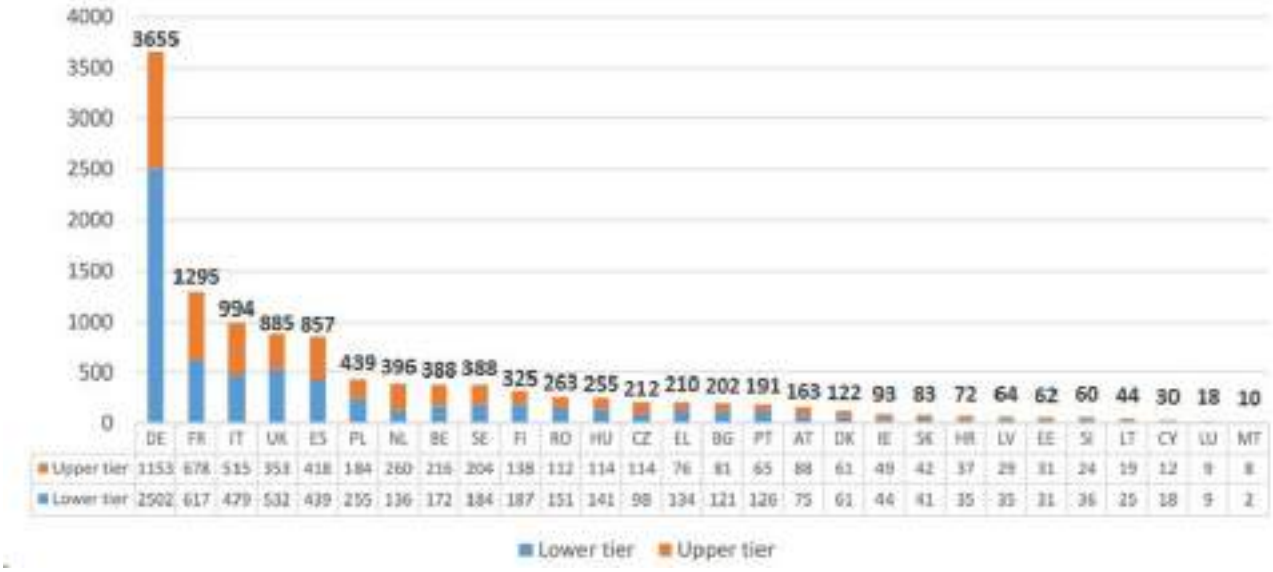

Figure 4: Number of Seveso establishments in 2018. Source: European Commission (2021).

Regarding the previous data, Italy ranked third among the Member States with a higher number of establishments, slightly above 8% of the European total. Considering more updated data, Italy owns 471 LTE and 507 UTE (ISPRA, 2023). Figure 5 offers the distribution of Seveso establishments in Italy, falling under different categories of activities belonging to the current Italian legal framework for Seveso establishments.

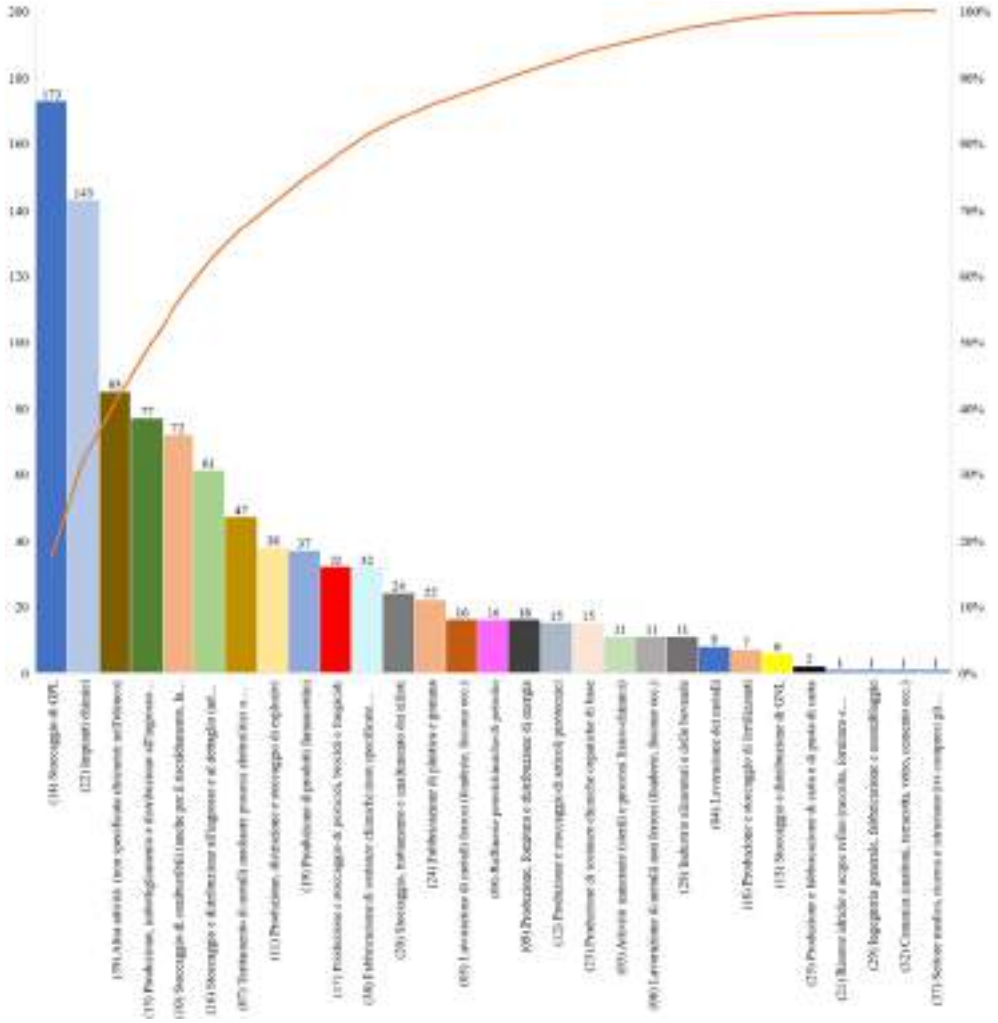

Figure 5: Distribution of different category activities for Seveso establishments categories in Italy. Source: ISPRA (2023).

Even if the previous image shows a horizontal axis in the original language (Italian), it could be appreciated that each category is preceded by a code between parentheses. These codes belong to 39 different defined activities typologies foreseen within the form of notification for Seveso establishment. It can be appreciated that activities such as (14) "liquefied pressurized gas (LPG) storage depots", (22) "chemical plants", (13) "LPG production, bottling, and wholesale distribution", (10) "fuel storage", (16) "production, bottling and wholesale distribution of fuels (excluding LPG)", collectively accumulate up to 50% of the total number of dangerous establishments in the country.

It is also curious, how the category (39) "other activities" presents several establishments whose activities are non-specified among the lists of 38 classifications. Due to the large number of plants within other activities (up to 8%), uncertainties arise in the decision-making given the functional heterogeneity (technology, hazardous substances, industrial macro-sector) of these plants located across the geography of the Italian country.

After this first glance to introduce the peculiarities of the Italian context concerning the major hazard industries (MHI) as a representative case study, it is crucial to discuss how the Italian framework on the control of major hazard Industries involving dangerous substances (see Legislative Decree No. 105 of June 26, 2015,

"Implementation of Directive 2012/18/EU on the control of major-accident hazards involving dangerous substances." Italian Official Gazette General Series No. 161 14/07/2015-Suppl. Ordinary No. 38).

3.2.b.1.3 Theoretical background model mutual vulnerability of industrial assets and their interaction with surrounding territories within a territorial multi-hazard context.

The concept of "resilience" is absent within the legal text of the D.Lgs. 105/15 and its enforcing regulations. Conversely, terms associated with the vulnerability concept were identified, predominantly linked to urban procedures connected with the land use planning (Ministry of Public Works Decree, 2001), or regarding the formulation, information, and experimentation of the external emergency plan (Minister for Civil Protection and Sea Policies, 2022). The categories of vulnerabilities mentioned within the Italian land use policies are considered just the sense where industry may impact the exterior environment (people in the damaged area, or critical environmental elements impacted). However, the analysis in the inverse sense where multiple natural hazards present in the territories where industries are located, might impact the industrial critical infrastructures (ICIs) is not contemplated (Pilone et al., 2017).

In addition, the legal procedures for the external emergency, although they recognize the association between natural factors and the occurrence of technological scenarios (NaTech scenarios), which in many cases, render ineffective the assumed response models in the emergency plans, these guidelines explicitly stated they cannot be utilized to plan for emergencies related to establishments with major accident hazards that result from events caused by natural risks. Consequently, there is still a lack of provisions in the transposed Italian legal framework for Seveso III to handle vulnerable ICIs considering the mutual impacts between industries and the multiple hazards inherent to their surroundings (Castro Rodriguez, 2024). In this regard, the function-location approach was conceptualized to address the current limitations (see Figure 6).

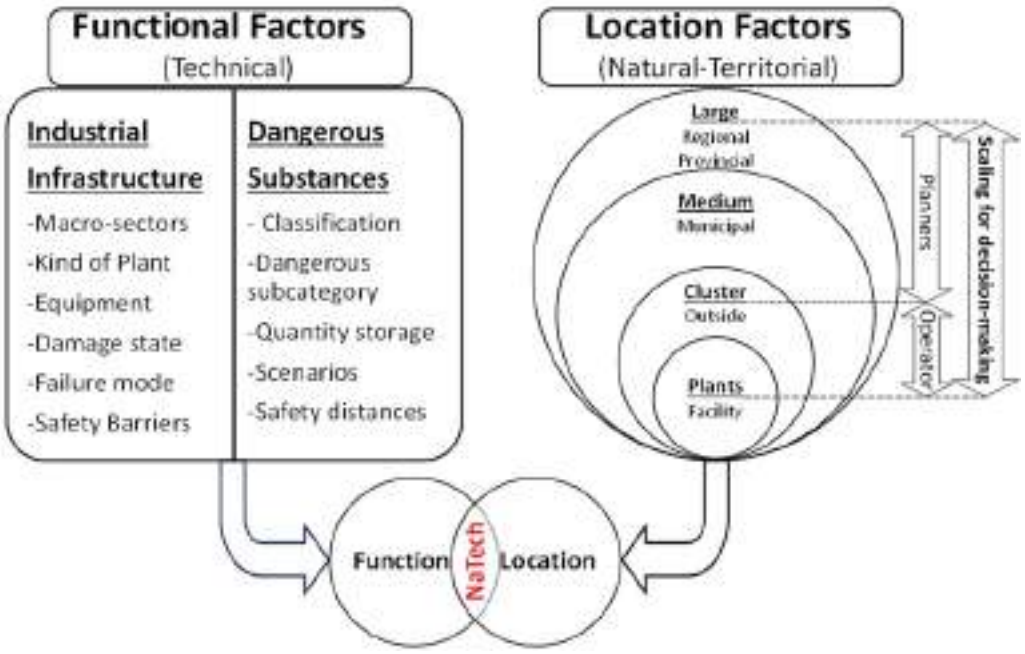

Figure 6: Function-Location approach to characterize NaTech vulnerabilities and support the decision-making process in industrial multi-hazard contexts.

The Figure 6 conceptualizes the occurrence of NaTech events (lower part of the image in red), as the potential result of intersecting factors dependent on the technical functionalities or attributes belonging to the ICIs, and multiple factors inherent to their surrounding location. Functional and location factors are further subdivided.

The left side, corresponding with functional vulnerabilities is categorized into "industrial infrastructure" and "dangerous substances." It is important to note that the possible categories of attributes for functional factors are not limited to those represented in Figure 6.

On the other hand, location factors (natural or territorial hazards) are represented at multiple scales and decision levels, reflecting the complexity of the legal system. Functional factors can be analyzed at various scales such as national, regional, provincial, municipal, or local. The local scale encompasses the industrial context within the facility fence line and the surrounding territory. This representation includes the interface where planners from public administration or different territorial governments (region, province, municipality) interact with industrial operators in a decision-making process with varying levels of authority and interests.

Specifically, the "location factors" on the right side of Figure 6 are developed by a comprehensive procedure for the "Spatial vulnerability characterization between industrial infrastructure and territory using a multi-hazard, multi-scale approach" which is represented in Figure 7.

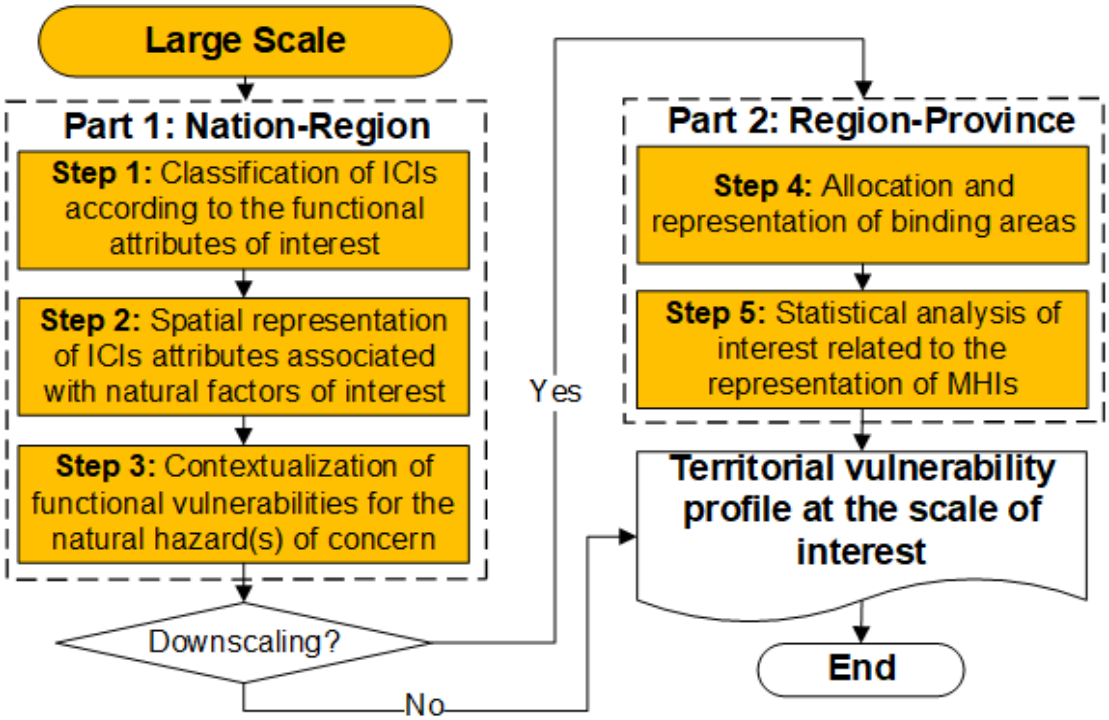

Figure 7: Place-based procedure for systematically characterizing the NaTech vulnerability of ICIs within a multi-hazard context at large scale.

3.2.b.2 Vulnerability assessment of drinking water and wastewater treatment plants as point critical infrastructures using a multi-hazard, multi-scale approach

3.2.b.2.1 .Contextualization of wastewater treatment plants in the European framework on the resilience of critical entities to the effects of extreme events, emphasized by climate change

Climate change is increasingly reshaping the frequency, magnitude, and characteristics of natural events, posing unprecedented challenges across the globe (Pilone et al., 2021). Rising global temperatures significantly contribute to the intensification of the water cycle, as higher temperatures increase the amount of atmospheric moisture available during storms. This accelerates and amplifies precipitation patterns, profoundly affecting both the spatial and temporal distribution of rainfall. As a result, extreme weather events such as torrential rains, severe storms, and prolonged droughts are becoming more frequent and intense, with cascading consequences for natural systems, human societies, and economies.

Europe has borne the brunt of some of the world's most devastating and costly natural disasters. Data from NatCatSERVICE (2010), which offers a reliable long-term dataset on disaster occurrences, highlights a clear upward trend in the frequency of disasters within Europe. This surge is closely linked to the escalating incidence of meteorological and hydrological events, such as floods, storms, and heatwaves (Figure 8). The implications of this trend are far-reaching, as disasters disrupt critical infrastructure, threaten public safety, and impose substantial financial and social costs on affected regions.

Climate change is already affecting, and will continue to significantly impact, all organizations, regardless of their size, type, or sector, in multiple ways and for decades to come.

These impacts will manifest in diverse ways, including disrupted operations, increased costs, and heightened risks to assets and workforce safety, making it imperative for organizations to adopt adaptive and resilient strategies for decades to come.

One particularly concerning consequence of natural disasters is the occurrence of Na-Tech (Natural-Technological) events. These are highly intense natural phenomena that simultaneously trigger cascading technological accidents within industrial or urban settings. Na-Tech events exacerbate the damage caused by the initial natural disaster and can have severe implications for human health, environmental integrity, and societal infrastructure.

The mechanisms underlying Na-Tech events involve the interaction of natural hazards -such as earthquakes, tsunamis, volcanic eruptions, floods, landslides, storms, tornadoes, and lightning- with industrial systems and facilities. This interaction can lead to catastrophic technological accidents, including fires, explosions, and the release of hazardous substances into the air, soil, and water systems. The impacts are far-reaching, affecting residential areas, public spaces, and critical economic activities such as production and commerce.

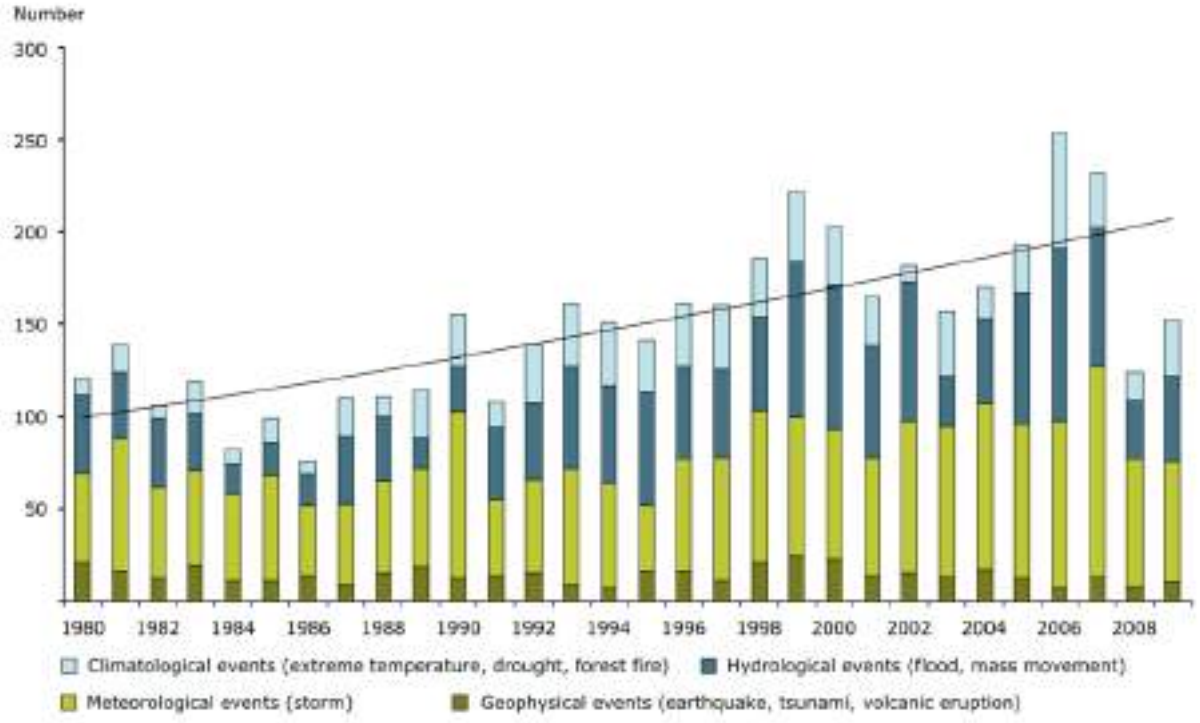

Figure 8: Disasters due to natural hazards in EEA member countries, 1980–2009 (NatCatSERVICE, 2010).

Therefore, to address the impacts of climate change, it is important to identify areas and objects that may be affected by these events (Masud and Khan, 2024).

Critical infrastructures constitute a central element of analysis. These are large-scale, man-made systems that function interdependently to produce and distribute essential goods. In particular, an infrastructure is defined as critical if its failure or destruction has a significant impact on health, environmental, safety, economic, and social well-being. They are generally built to exist over long periods, which means elements will be exposed to both rapid-onset (e.g., storm surge) and slow-onset (e.g., sea level rise) events.

For this reason, their response to climate change is of utmost importance (Shakou et al., 2019).

Water treatment infrastructures like wastewater treatment plants (WWTPs) and drinking water treatment plants (DWTPs) are critical infrastructures as they are essential for ensuring the public health of the community.

3.2.b.2.2 Theoretical background model mutual vulnerability of wastewater treatment plants and their interaction with surrounding territories within a territorial multi-hazard context

As mentioned before, European Commission issued Directive (EU) 2022/2557 on the resilience of critical entities requiring Member States to identify and assess their risk, emphasizing the influence of all natural events in incidents.

In water treatment plants, the effects are often related to the loss of functionality (Casson Moreno et al., 2018). Extreme weather can interrupt the services and treatment efficacy of water infrastructures, leading to the discharge of untreated or insufficiently treated wastewater into the natural environment (Labonté-Raymon et al., 2020). To mitigate these impacts, a throughout knowledge of the combined effects of such events is an essential first step to improve WWTPs and DWTPs resilience. However, literature concerning the adaptation of critical infrastructures to climate change and natural disasters is just emerging.

In this work, vulnerability assessment and detection of signals within multi-hazard contexts where wastewater treatment plants are located is the first part of operationalizing resilience, considering the theoretical concepts defined by (Castro Rodriguez, 2024). It is specified that the mapping procedure and subsequent considerations were the same in the case of DWTPs as well.

In order to estimate the effects of extreme events it is certainly important to identify areas (LOCATION) and related infrastructures (FUNCTION) that may be damaged by these events. Therefore, the function location approach defined by (Castro Rodriguez, 2024) has been fitted to wastewater treatment plants as a case study (Figure 9).

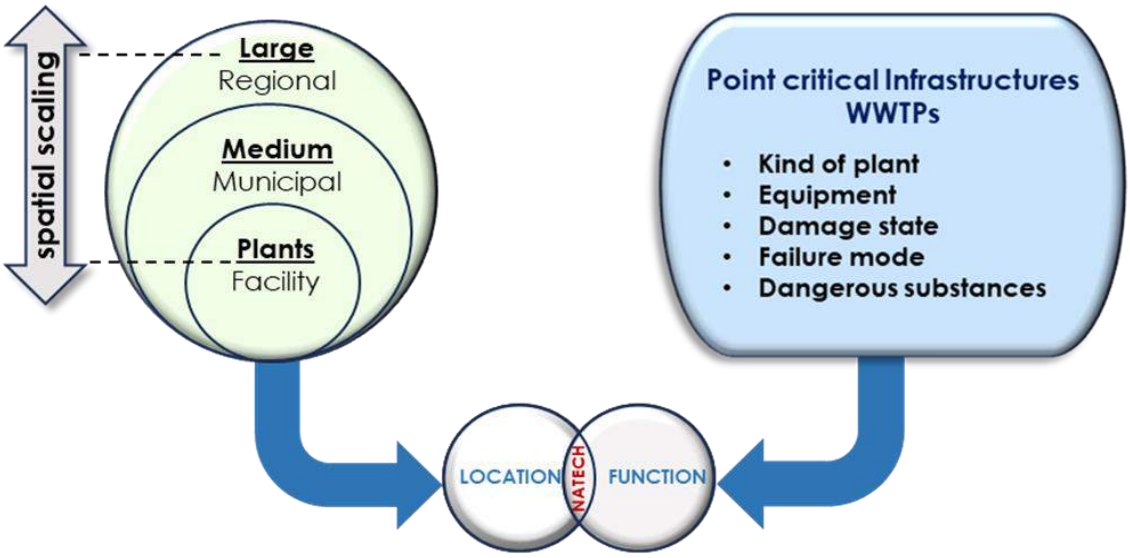

Figure 9: Function-Location approach tailored to wastewater treatment plants.

In this case, the left side of the analysis framework is defined by the location factor, which refers to natural or territorial hazards that occur at different scales and inform decision-making across various levels. On the right side, the focus shifts to the functional factor, which pertains to the characteristics and operations of industrial plants. Both factors can be analyzed at multiple levels, including national, regional, provincial, municipal, and local scales. At the local level, the analysis narrows in on the industrial context within the plant's boundaries and the surrounding territory, offering a more granular perspective on risks and interactions.

The functional factor focuses on the plants themselves and has been assessed through detailed mapping at the national and regional levels. At the national scale, the distribution of wastewater treatment plants was visualized using a color-coded system to represent variations in density and capacity across the country. This mapping relied on data from the 2015 ISTAT database, providing a broad overview of plant locations. The analysis was then refined at the regional level with precise location data for individual plants, enabling a closer examination of their geographical positioning and interactions with specific regional characteristics. This dual-level approach ensures that both large-scale trends and localized details are accounted for.

On the other hand, the location factor addresses external hazards and their impact on industrial infrastructure. This aspect was developed through a comprehensive procedure for characterizing spatial vulnerability between industrial facilities and their surrounding territories, utilizing a multi-hazard and multi-scale approach. The methodology considered four key types of natural hazards: coastal risks such as erosion and storm surges; hydraulic threats including flooding and river overflow; geomorphological vulnerabilities like landslides and soil instability; and seismic hazard associated with earthquakes. These hazards were evaluated systematically at the national level to identify broader patterns of vulnerability and exposure. The analysis was then focused at the regional level and finally at the scale of individual plants, ensuring that site-specific vulnerabilities were thoroughly assessed.

By integrating the functional and location factors, this framework offers a holistic perspective. The multi-scale methodology ensures that vulnerabilities are examined comprehensively, from overarching national trends to the detailed, localized challenges faced by individual facilities. The analysis captures how plant-specific characteristics intersect with territorial hazards. This detailed understanding allows for a nuanced evaluation of cascading risks, where the vulnerability of industrial plants can amplify the impacts of natural hazards on nearby communities and ecosystems.

This dual-factor approach provides valuable insights for stakeholders at all levels. It enables decision-makers to prioritize interventions, allocate resources effectively, and enhance the resilience of industrial facilities to natural hazards in an increasingly complex risk landscape (Figure 10).

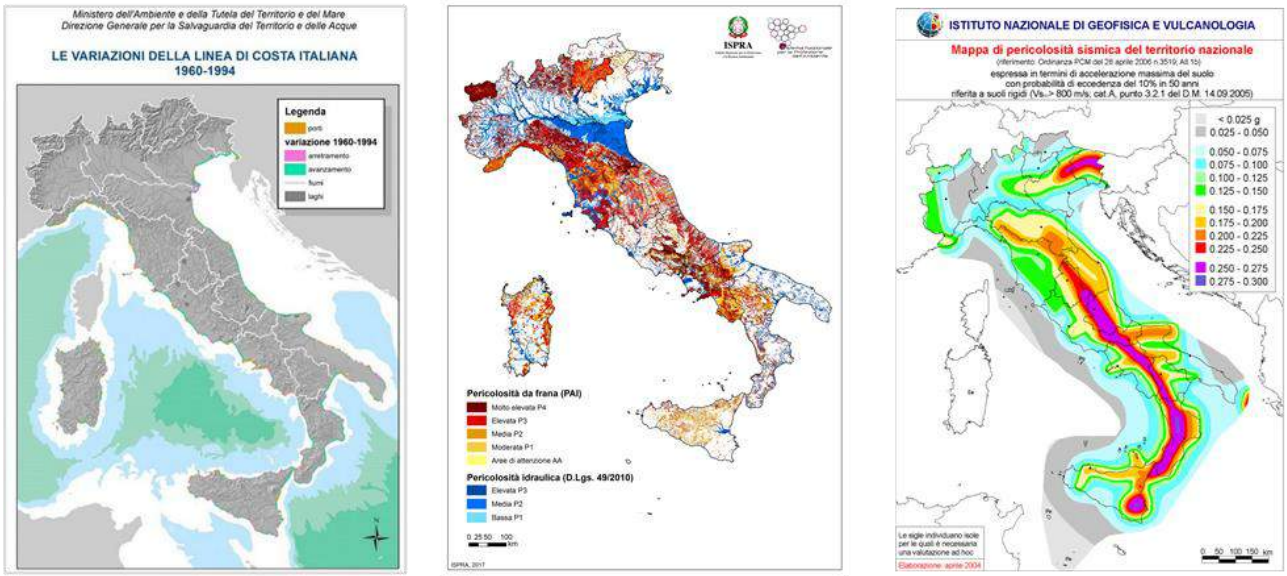

Figure 10: National-level mapping of coastal, hydraulic, geomorphological, and seismic hazards.

3.2.b.2.3 Multi-hazard and multi-scale approach tailored to WWTPs and DWTPs

Focusing on the Sicilian region, each hazard map was harmonized so that H_1 corresponded to the lowest hazard and H_4 corresponded to the highest. The harmonization of maps allows all hazard zones to be converted into a common format to facilitate comparison, as their definitions generally vary between different maps. Harmonization ensures that hazards are uniformly defined and classified so they can be overlaid, enabling the identification of areas with cumulative hazards (Figure 11).

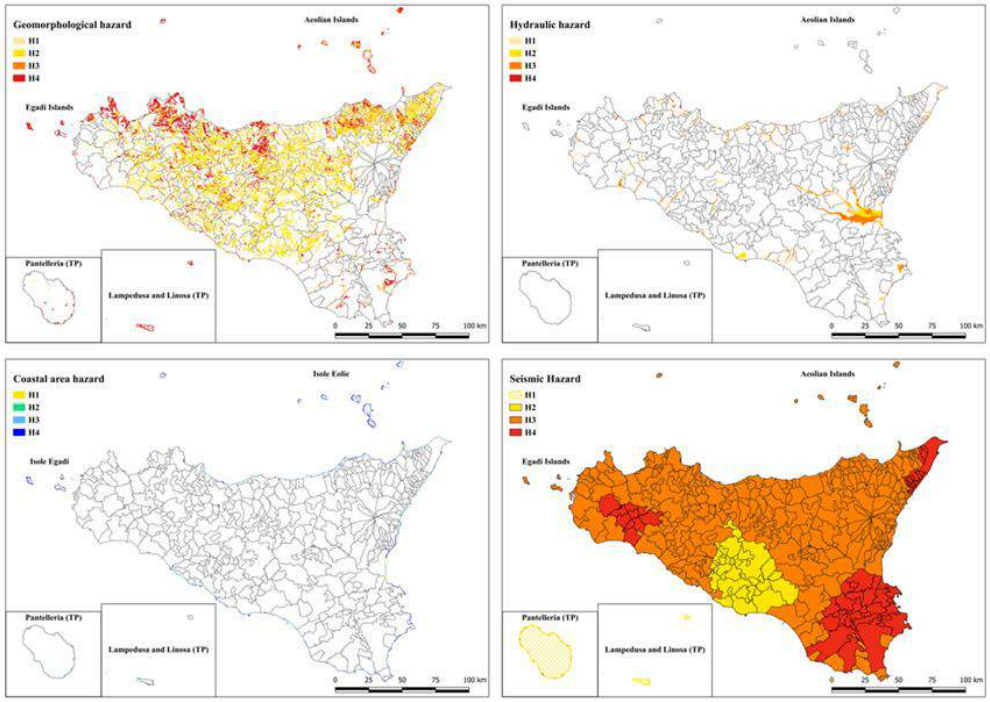

Figure 11: Regional-scale mapping of coastal, hydraulic, geomorphological, and seismic hazards after harmonization of classes.

Hereafter, a multi-hazard GIS-analysis was applied. The Sicilian territory was divided into a grid with 200 m x 200 m cells. Each cell is identified by an index i. Specifically, the harmonized classes H_k (k = 1, 2, 3, 4) were assigned the following numerical values: H_1 = 0,25; H_2 = 0,5; H_3 = 0,75; H_4 = 1; thereby transitioning from a qualitative to a quantitative classification.

As mentioned before, four hazard types j are considered:

- Seismic hazard ($j = s$)
- Geomorphological hazard ($j = g$)
- Hydraulic hazard ($j = h$)
- Coastal hazard ($j = c$)

Each cell i is composed of portions that may belong to different hazard classes. The total area of the cell is denoted as A_i (40000 m^2), while the area of the portion of territory associated with class H_k for hazard j is $A_{i,j,k}$.

For every cell, the relative weight of each hazard class is determined by the proportion of the cell's area associated with that class, given by

$$W_{i,j,k} = \frac{A_{i,j,k}}{A_i} \tag{3.2.11}$$

This weight quantifies how much each class contributes to the overall hazard in the cell. To calculate the contribution of a specific class, we multiply its relative weight by its assigned numerical value H_k.

Summing these contributions across all classes, we obtain the individual hazard indicator for hazard j within cell:

$$HI_{i,j} = \sum_{k=1}^{4} (W_{i,j,k} \cdot H_k) \tag{3.2.12}$$

This process is repeated for each type of hazard j.

The calculation of the individual hazard indicator is based on a weighted summation of the hazard classes within the cell. This method can be interpreted as an approximation of an integral over the cell's surface, where the integrand represents the hazard level.

Finally, the multi-hazard index for cell i is computed as the weighted sum of individual hazard indicators, with unit weights for each hazard:

$$MHI_i = \sum_{j \in (s,g,h,c)} HI_{i,j} \tag{3.2.13}$$

A multi-hazard map was created to classify the territory into four distinct hazard levels, representing a gradation of potential threats. The classes are defined based on thresholds of the Multi-Hazard Index (MHI), which quantifies cumulative hazard levels. The thresholds are as follows:

- Class 1 (Low Hazard): $0 \leq MHI < 0.30$
- Class 2 (Moderate Hazard): $0.30 \leq MHI < 0.60$
- Class 3 (High Hazard): $0.60 \leq MHI < 0.90$
- Class 4 (Very High Hazard): $MHI \geq 0.90$

These classes range from low to moderate hazards, extending to medium-high hazards. The classification was carefully designed to provide a clear framework for assessing and communicating risks in a structured and actionable manner. Additionally, these hazard maps were overlaid with the locations of wastewater treatment and drinking water treatment plants. This integration allowed for a detailed evaluation of the vulnerability of these critical facilities to the identified hazards. By combining the hazard classification with the spatial distribution of water infrastructure, the study provided insights into which plants are most at risk, enabling the development of targeted strategies to enhance their resilience. This approach ensures that resources are allocated efficiently to safeguard essential services and public health.

3.2.c Coastal flooding caused by tsunami waves generated by earthquakes

3.2.c.1.1 Introduction

Tsunamis have caused large destruction on coastal communities and ecosystems (Koshimura and Shuto, 2015; Mori et al., 2011; Synolakis and Kânoğlu, 2015). These phenomena are generated by other natural events such as earthquakes (Tanioka and Satake, 1996), landslides, volcanic eruptions, atmospheric pressure disturbances (in this case they are referred to as "meteotsunamis"), and occasionally asteroid impacts (Grezio et al., 2017). Tsunami waves are characterized by long time periods ranging from minutes to hours, with wavelengths significantly larger than the water depth where they propagate. Due to this characteristic, tsunami waves are typically unnoticed offshore but become very destructive near the coast, particularly in marine bays or ports, where significant shoaling and energy concentration effects can occur (Röbke and Vött, 2017). Indeed, tsunami hazard is not primarily driven by the wave height (as is the case for wind-generated waves) but rather by the wave length λ. Upon reaching the shore, these waves often induce severe flooding potentially causing considerable damage (Bernard et al., 2006; Synolakis and Bernard, 2006; Titov and Synolakis, 1997).

The need for updated methodologies to assess tsunami hazard and risk became urgent after two of the most powerful seismic generated tsunamis in history the 1896 event in the Sanriku region of Japan and the 1946 event in the Aleutians (Kanamori, 1972; Tanioka and Satake, 1996), and later the 2004 event in the Indian Ocean, which resulted in approximately 290,000 human losses (Lay et al., 2005; Titov et al., 2005) and the most recent 2011 Tohoku event in Japan which affected many areas of the Pacific Ocean (Mori et al., 2011). The intensity of earthquakes and their frequency of occurrence have a primary role in estimating the tsunamigenic potential subsequent to an event allowing these estimations to be a foundational components of tsunami hazard and mitigation tools (Bernard and Titov, 2015; Dunbar et al., 2008; Kanamori, 1972). In this context, hazard assessment commonly involves quantifying the likelihood of exceeding a physical tsunami intensity parameter, e.g. the run-up elevation at a particular coastal site within a defined time period.

Risk assessment, on the other hand, incorporates hazard considerations alongside exposure factors, such as population density within a designated area, and the vulnerability characteristics of that area (Løvholt et al., 2022). In general, to mitigate tsunami risk three main types of actions are employed: i) pre-emptive actions; ii) almost simultaneous actions; iii) subsequent actions. Point i) is essential and at the basis of point ii) and point iii) and it is usually carried out using hazard assessment (Arcas and Uslu, 2010; Bernard et al., 2006). Due to these studies based on probabilistic frameworks and more specifically focusing on Probabilistic Tsunami Hazard Assessment (PTHA) (Geist and Parsons, 2006; Grezio et al., 2017; Lin and Tung, 1982), are increasingly common and becoming essential for planning risk reduction, which significantly helps in saving lives and reducing economic losses. Generally, PTHA methods are aimed at defining tsunami intensity parameters (e.g. wave amplitude a, wave height H, Maximum Inundation Height MIH at a prescribed distance from the coast, to assess the hazard of a certain coastal stretch starting from the tsunami genesis by analysing the tsunamigenic potential of the area under investigation (Anita et al., 2012; Cecioni et al., 2023; Lorito et al., 2015; Sørensen et al., 2012). The propagation inshore of these parameters is usually simplified and does not consider specific local bathymetry features except for a limited number of a specific case studies which are also expanded to analyse tsunami inundation (González et al., 2009; Lynett et al., 2013; Yuan et al., 2021). It should be stressed that, these approximations might not always be cautelative, and more refined numerical models are needed to obtain high-resolution results (Tonini et al., 2021).

3.2.c.1.2 TSUMAPS-NEAM project and simplified ISPRA inundation maps

Focusing on earthquake-generated tsunamis, the seismic-PTHA (sPTHA) database NEAMTHM18 (Basili et al., 2021) was recently developed as part of the European project TSUMAPS-NEAM led by INGV (Istituto Nazionale di Geofisica e vulcanologia - National institute for geophysics and volcanology) covering the coasts of the North-Eastern Atlantic, the Mediterranean Sea, and connected seas, (a basin referred to as NEAM) and providing probabilistic hazard curves in a very extensive coverage area. The coast is mapped

using different Points Of Interest (POIs) every 20 km and assigning to each one a set of hazard curves, defined with the percentile of the epistemic uncertainty, defining the values of the intensity parameter chosen MIH for a varying probability of occurrence with a fixed 50 years exposure time V_n. The MIH was calculated, after the initial generation and propagation offshore, using, close to the coast, amplification factors (Glimsdal et al., 2019) defined by carrying out linear 1D propagation towards the shore of signals with wave periods T between 120 s and 3600 s, which are typical of tsunamis (Basili et al., 2021).

Due to their entire coverage of the European coasts, the results of this project are being increasingly used by e.g. government agencies. In particular, the Italian Institute for civil protection and environmental research (Istituto superiore per la protezione e la ricerca ambientale - ISPRA) was tasked by the SiAM (Sistema di Allertamento nazionale per i Maremoti generati da sisma - National alert system for earthquake tsunamis) government directive in 2017 (DPCM, 2017) and in 2018 (Presidenza del Consiglio dei Ministri - Dipartimento della Protezione Civile , 2018) to create inundation maps of the entire Italian coast starting from NEAMTHM18 results (available at http://sgi2.isprambiente.it/tsunamimap). Due to the large coverage area involved, the very simplified approach described in (Tonini et al., 2021), which did not include inundation physics but defined the run-up as $R* = 3MIH + 1$ and used a DTM to define the inundation maps, was applied with the objective of designing them for evacuation routes and civil protection purposes. Even though the process for defining these inundation maps is very simplified they are also starting to gain a certain relevance for design projects of strategic infrastructures. However, in this case high-resolution simulations that consider the variably of the coast and consider both inundation depth over time and flow velocity over time are a necessity (Tonini et al., 2021) to e.g. use design guidelines such as ASCE (2022), CNR (2018) and FEMA (2012) to calculate impact forces onto structures or consider non-linear effects during a possible event. Even if the NEAMTHM18 is a powerful tool which maps tsunami hazard for the entire NEAM region, it lacks a specific methodology to transform the synthetic hazard parameter provided in inputs for high-resolution coastal inundation numerical simulations. The methodology presented herein addresses this issue and it can be easily extended to any coastal stretch in the NEAM region or to other PTHA databases.

3.2.c.1.3 Objectives

This study aims at addressing the lack of a clear methodology for applying NEAMTHM18 in any coastal stretch of the NEAM region, to allow high-resolution hazard assessment of an interest area. Therefore, the main objective of this study is to provide a new methodology generally applicable to any PTHA database to define inputs for high-resolution simulations of tsunami inundation. This methodology is an important link with the initial PTHA tool (e.g. NEAMTHM18) so that all the statistical parameters and studies undertaken while developing a PTHA are not set aside but rather used as a starting point when implementing new local tsunami inundation simulations. This will enable coastal engineers and government authorities to consistently use these tools to assess tsunami inundation risk with higher detail. Furthermore, the present study might also be of help to future developers of PTHA tools in better understanding what the end user needs for applying them in detailed studies.

3.2.c.2 Methodology

3.2.c.2.1 Introduction

Tsunami hazard assessment is critical for design plans that include coastal risk management, especially in seismically active regions. Appropriate evaluation is essential to develop and implement effective mitigation strategies for design projects. This section presents the developed methodology that uses the results from the NEAMTHM18 as input for high-resolution tsunami inundation simulations designed for engineering applications. As previously specified, *MIH* is the only available parameter for understanding the magnitude of a potential tsunami impact. To reach the objectives of this study and to streamline the entire methodology process three main methodological steps were defined:

- define the hazard by choosing a design exceedance probability leading to a design *MIH*;
- define the incident tsunami scenarios to be simulated choosing in the range of periods used in NEAHMTHM18;

- carry out high-resolution simulations with the objective of producing hazard maps of an area of interest or time-varying variables for a specific infrastructure.

The following section will provide a detailed description of each step of the methodology, offering comprehensive guidance for implementing this approach in coastal risk management projects.

3.2.c.2.2 Hazard intensity parameter - MIH

The NEAMTHM18 database was used. Therefore, the hazard intensity parameter adopted is the *MIH*, which is defined through hazard curves at different POIs positioned along the coasts of the NEAM region at water depths of h = 50 m (Figure 12). This parameter is defined as the maximum height reached by the water during a seismic tsunami inundation (Glimsdal et al., 2019). Fig. 12 defines all the parameters for a generic transect analysed in the NEAMTHM18 sPTHA, with *MSL* the mean sea level and *R* the maximum run-up of the inundation.

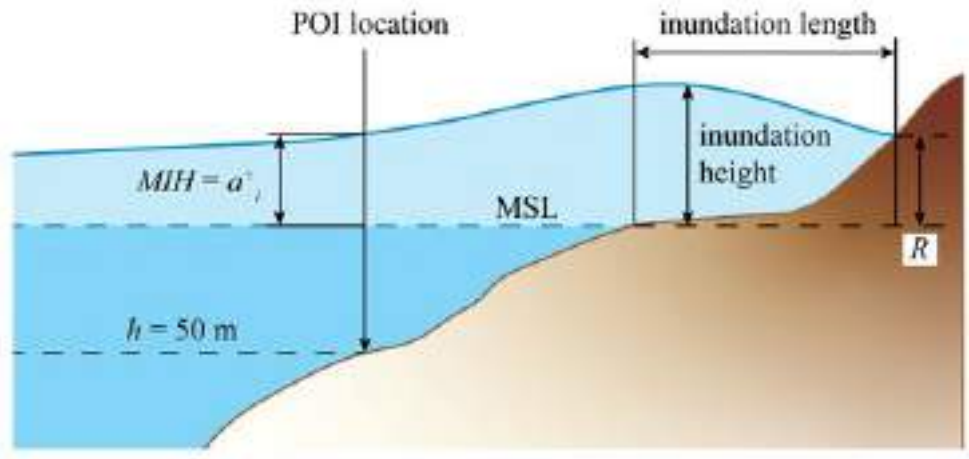

Figure 12: Sketch of relevant variable in a sample transect of a single POI location.

Hereinafter, an approximation was applied by assuming the relationship *MIH* = positive amplitude of the incident tsunami (a_i^+) at the position of the POI (h = 50 m). This approach was chosen due to the need for a methodology that can be also applied for engineering application during design project of strategic structure or infrastructure. This will simplify the definition of the incident tsunami amplitude but allowing the inclusion of proper overland inundation physics using the appropriate numerical models. This, in turn, will allow for a more physics-oriented modelling than what is available through the current inundation maps for the NEAM region. Different approaches such as backward propagation might be also applied as MIH location is not known a priori for each transect due to the high variability of the coast alongshore and cross-shore. However, since NEAMTHM18 information are given every 20 km this might still be very prone to under/overestimations.

3.2.c.3 STEP 1 - Definition of the design hazard indicator

The first important part of the present methodology is the definition of the hazard by setting an exceedance probability P_{vr} for the area of interest that together with V_n and the epistemic uncertainty percentile will, in turn, allow to define the design Maximum Inundation Height MIH_d for the specific application. Due to each POI being at around 20 km distance from each other the final MIH_d is then selected as the highest value of all hazard curves, for a fixed percentile, at the POIs in a 40 km radius circumference around the interest area. This procedure was described in Tonini et al. (2021) and applied for the Italian inundation maps. The exceedance probability P_{vr} (Kottegoda and Rosso, 2008) of the design Maximum Inundation Height MIH_d to be exceeded for a fixed average return period *ARP* of the earthquake can be defined as:

$$P_{vr}(MIH \geq MIH_d) = 1 - \left(1 - \frac{1}{ARP}\right)^{V_n} \quad (3.2.14)$$

Note that, the temporal window of exposure time for the NEAMTHM18 database is V_n = 50 y.

The DPCM (2017) set for the Italian coasts an *MIH* defined with an *ARP* = 2500 y and a hazard curve with an epistemic uncertainty at the 84th percentile resulting (with the fixed V_n = 50 y) in a $P_{vr} \approx 2\%$. However, the curves defined in NEAMTHM18 can also be applied for different values of V_n by calculating an equivalent probability of exceedance P_{evr}. This is done first by fixing the probability of exceedance and the exposure time and using:

$$ARP = -V_n / \ln(1 - P_{vr}) \tag{3.2.15}$$

Eq. 3.2.14 can be applied again with the calculated *ARP* but V_n = 50 y to find the new Pe_{vr}. For example, considering P_{vr} = 2% and V_n = 100 y and applying Eq. 3.2.15 *ARP* = 5000 y, then Eq. 3.2.14 can be used to calculate Pe_{vr} = 1% which is equivalent to a P_{vr} = 2% with V_n = 100 y. Additionally, thanks to the close connection between earthquakes and tsunamis generated by them, the use of P_{vr} values prescribed by design standards for structures in seismic areas such as the Italian (NTC, 2018), can also be envisaged. Here, P_{vr} depends on the final allowed damaged state of a structure and it is a good and the only option to correlate tsunami hazard to earthquake hazard in a structural design context in Italy.

Finally, after defining the MIH_d, the approximation $MIH_d = a_i^+$ is applied so that STEP 2 can be used to define a set of incident tsunami scenarios.

3.2.c.4 STEP 2 - Define the incident tsunami scenarios

STEP 2 represents the core of the developed methodology and for this reason a flow chart is represented in Figure 13 to streamline the process and simplify the application of the proposed methodology. STEP 2 starts once the hazard intensity is defined in STEP 1 and ends with STEP3, which focuses on the 3D tsunami inundation simulations.

Due to the potentially infinite possible signals that could be generated during real events and to reduce the number of simulations to a reasonable number for engineering purposes the range of considered wave periods *T* is chosen between 120s and 3600s, following NEAMTHM18 (Basili et al., 2021) in which it is considered a reasonable range for this phenomenon. Additionally, a subset of a discreet number of scenarios should be chosen considering the coast characteristics in the area of interest. First, using the chosen set of *T* to be analysed and applying the shallow water theory the mild slope condition is checked on the offshore bathymetry of the chosen POI. This condition needs to be verified in order to be able to generate a waveform appropriate to the local conditions and to correctly apply the chosen wave theory. If this condition is not verified at the POI the tsunami boundary condition needs to be moved offshore at suitable depth where this condition is met or until a possible tsunami seismic source is found.

After the previous procedure is concluded by using the chosen *T*, final local *h* and initially considering *H* at the generation point as *H* = 0.001h (Tadepalli and Synolakis, 1996) the most appropriate wave theory to be applied is estimated. Since in the literature the N-WAVE (Madsen et al., 2008; Madsen and Schäffer, 2010) theory is known to be representative of seismic tsunamis free water surface elevation in time and space, the present methodology focuses on this particular theory. It should be noted that for specific cases other theories might also be appropriate e.g. in cases where frequency dispersion has developed in a consistent way due to the long travelling distance of the tsunami. This would result in a wave form closer to a simple harmonic wave rather than an impulsive one (Madsen et al., 2008). The N-WAVE water surface variation in time and space in a fixed h can be written following (Veloso Lima et al., 2019) extension of Tadepalli and Synolakis (1996)

$$\eta(x,t) = \epsilon(\theta - \kappa\delta) H \operatorname{sech}^2\theta \tag{3.2.16}$$

where ϵ is a scale factor to define the wave height as *H*; $\epsilon < 0$ results in a leading depression (LD) N-WAVE while for $\epsilon > 0$ a leading elevation (LE) N-WAVE is obtained. $\delta = x_2 - x_1$ is a parameter the allows a changing position of the inflection point where $x = x_2$ is its location and $x = x_1$ is the position of the crest of a solitary wave of the same *H* and wavelength λ of the N-WAVE. For $\delta = 0$, Eq. 3.2.16 generates an isosceles N-WAVE for which $a^+ = a^- = H/2$. θ is defined as

$$\theta = \kappa(x - ct - x_1) \tag{3.2.17}$$

where $c = \sqrt{g(H + h)}$ is the solitary wave celerity and the wave number κ is defined following (Tadepalli and Synolakis, 1996)

$$\kappa = \sqrt{\frac{p_0 3H}{4h^3}} \tag{3.2.18}$$

where p_0 is wave a steepness parameter, which, in turn, regulates the effective wave period which for a solitary or an N-WAVE wave can be calculated as

$$T_{eff} = \frac{2\pi}{\kappa c} \tag{3.2.19}$$

To apply the described theory for each fixed *T*, two different conditions might verify depending on the area of interest (Figure 13): (I) the offshore boundary condition is placed at h = 50 m or (II) the offshore boundary condition is at h > 50 m. If (I) is verified then $MIH_d = a_i^+$ is already true and the N-WAVE theory can be directly applied to calculate the inputs for the 3D inundation simulations of STEP 3. However, if (II) is verified 2DV numerical simulations are used to propagate the tsunami signals between the offshore boundary point with h > 50 m and the POI point (h = 50 m) avoiding shore reflection so that the final signal only includes the incident wave. Note that in (II) being h > 50 m the amplitude at this location should be $a2+ < a_i^+$ since shoaling tends to increase the tsunami H and $MIH_d = a_i^+$ needs to be verified at h = 50 m. Once $MIH_d = a_i^+$ is verified the new final obtained time series can be then used in STEP 3.

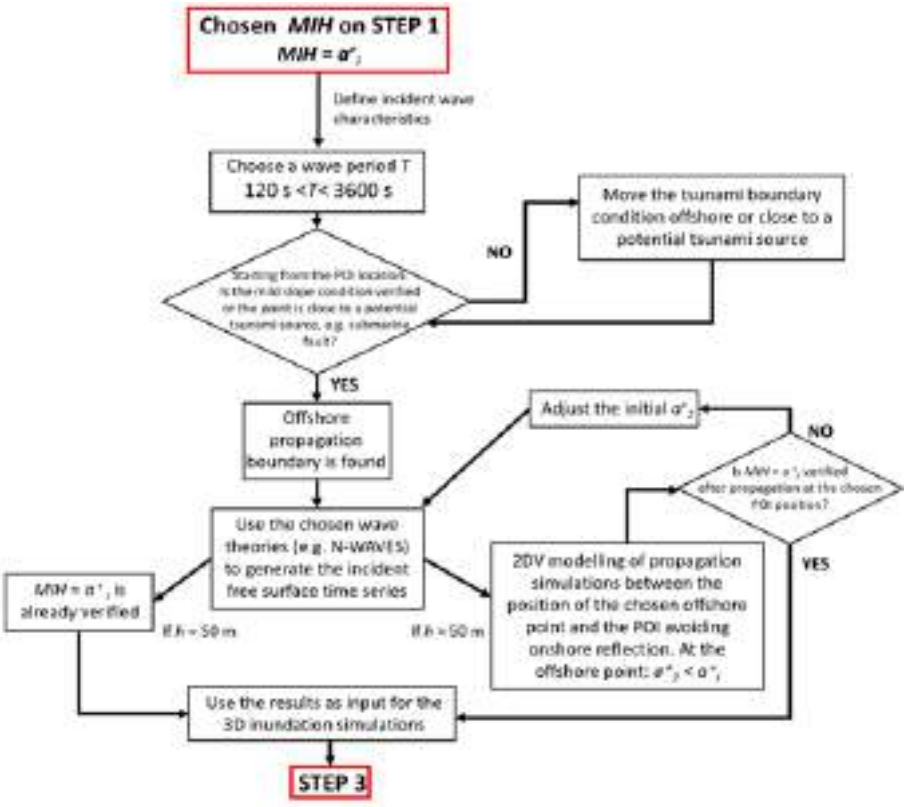

Figure 13: Flow chart for STEP 2 of the developed methodology.

3.2.c.5 STEP 3 - High resolution inundation simulations and hazard mapping

The incident time series of the set of tsunami scenarios defined in STEP 2 are used in STEP 3 as boundary conditions for high-resolution 3D inundation simulations starting from an offshore water depth of h = 50 m (corresponding to the h of every POI in NEAMTHM18 database where $MIH_d = a_i^+$ is assumed). Simulations are carried out for each chosen boundary condition. Particular attention should be put into defining both the bathymetry and topography of the area of interest at this stage by necessarily using high-resolution datasets that are able to correctly capture the particular configuration of the coast that could enhance or diminish the tsunami inundation hazard. Additionally, for simulations of smaller areas,

structures buildings might be physically added as fixed object or an approach relying on a variable friction coefficient to simulate them might be used (Kaiser et al., 2011; Oishi et al., 2015).

Once the entire set of scenarios is simulated the numerical results can be:

- extrapolated from each or specific computational cells for a time series of a measured variable such as the free water surface η or the flow velocity magnitude v;
- aggregated to evaluate the cumulative hazards of all simulations for e.g. maximum inundation depth and maximum velocity with the goal of developing high-resolution hazard maps of the area of interest.

In the following section, the numerical model used by the authors to apply the developed methodology is introduced. However, it must be noted that any numerical model relying on similar governing equations and that allows for wetting and drying of the emergent land can be equally applied.

3.2.c.6 Numerical model for tsunami offshore propagation and inundation

Tsunami wave signals propagation and inundation was carried out using SWASH (Simulating Waves till Shore) numerical model (Zijlema et al., 2011). SWASH is an open-source numerical model based on the Non-Hydrostatic Non Linear Shallow Water Equations (NH-NLSWE) developed by the University of TUDelft.

SWASH model is a non-hydrostatic numerical model designed to simulate wave dynamics, including tsunami propagation and inundation, with high accuracy and efficiency. Contrary to Boussinesq-type wave models, based on higher-order derivative terms to improve the dispersion characteristics, nonhydrostatic models improve their frequency dispersion by increasing the number of grid points or vertical layers rather so they contain at most second-order spatial derivatives (Zijlema and Stelling, 2008).

By solving the nonlinear shallow water equations with vertical momentum and non-hydrostatic pressure terms, SWASH effectively captures both nonlinear effects and dispersive wave characteristics, critical for modeling tsunamis as they transform and interact with coastal areas. The model employs a compact difference scheme combined with a vertical terrain-following grid, ensuring efficient and accurate representation of frequency dispersion with relatively few vertical layers. A key feature of SWASH is its robust wet-dry algorithm, which dynamically tracks the moving shoreline without introducing numerical instabilities. This capability is essential for accurately simulating processes like inundation, wave run-up, and overtopping. The model uses an upwind scheme for calculating momentum flux, ensuring numerical stability when transitioning between wet and dry areas, such as during wave run-up. This approach prevents oscillations or instabilities that could occur in regions with rapidly changing water depths. The shoreline is not fixed but moves dynamically as waves interact with the coast (e.g., during wave run-up or overtopping). The model uses a simple tracking method to determine the position of the moving shoreline at every time step. This is crucial for accurately simulating processes.

The governing equations concern mass and momentum conservative nonlinear shallow water equations in Cartesian coordinates (x, y) considering depth-averaged, non-hydrostatic, free surface flow. The domain is bounded vertically by the free surface $z = \eta(x, t)$ and the bottom $z = -d(x)$. Consequently, the total water depth is $h(x, t) = \eta(x, t) + d(x)$.

Summarising the governing equations, they are represented by the NLSWE that can be derived from the Navier-Stokes equations for an incompressible fluid in a 2DH depth average flow:

$$\frac{\partial \eta}{\partial t} + \frac{\partial hu}{\partial x} + \frac{\partial hv}{\partial y} = 0 \tag{3.2.20}$$

$$\frac{\partial u}{\partial t} + u\frac{\partial u}{\partial x} + v\frac{\partial u}{\partial y} + g\frac{\partial \eta}{\partial x} + \frac{1}{h}\int_{-d}^{\eta}\frac{\partial q}{\partial x}\,dz + c_f\frac{u\sqrt{u^2+v^2}}{h} = \frac{1}{h}\left(\frac{\partial h\tau_{xx}}{\partial x} + \frac{\partial h\tau_{xy}}{\partial y}\right) \tag{3.2.21}$$

$$\frac{\partial v}{\partial t} + u\frac{\partial v}{\partial x} + v\frac{\partial v}{\partial y} + g\frac{\partial \eta}{\partial y} + \frac{1}{h}\int_{-d}^{\eta}\frac{\partial q}{\partial y}\,dz + c_f\frac{v\sqrt{u^2+v^2}}{h} = \frac{1}{h}\left(\frac{\partial h\tau_{yx}}{\partial x} + \frac{\partial h\tau_{yy}}{\partial y}\right) \quad (3.2.22)$$

$$\frac{\partial w_s}{\partial t} = \frac{2q_b}{h} - \frac{\partial w_b}{\partial t} \quad (3.2.23)$$

$$w_b = -u\frac{\partial d}{\partial x} - v\frac{\partial d}{\partial y} \quad (3.2.24)$$

$$\frac{\partial u}{\partial x} + \frac{\partial v}{\partial y} + \frac{w_s - w_b}{h} = 0 \quad (3.2.25)$$

in which Eq. 3.2.20 represents the mass conservation equation and Eqs. 3.2.21 and 3.2.22 represent the momentum equations in a non-conservative form. Introducing the velocity in z-direction at the free surface w_s and at the bottom w_b, it is possible to define the vertical momentum equations as Eqs. 3.2.23 and Eq. 3.2.24. Consequently, the local conservation of mass can be written as Eq. 3.2.25. In Eqs. 3.2.24 and 3.2.25:

- t is time;
- x,y are located at the still water level;
- $u(x, y, t)$ and $v(x, y, t)$ are the depth average velocity components in x and y directions;
- w_b and w_s represent the velocity in z-direction at the bottom and at the free surface respectively;
- g is the gravity acceleration;
- $q(x, y, z, t)$ is the non-hydrostatic pressure with $q(x, y, z, t)|_{z=\eta} = 0$;
- c_f is the dimensionless bottom friction coefficient and τ_{xx}, τ_{yy}, τ_{xy} and τ_{yx} represent the horizontal stress terms.

The extension of the presented set of equations to a 3D framework, used for the simulations in the present study, can be extrapolated from Zijlema and Stelling (2008).

To prevent wave re-reflections at the offshore boundaries, a weakly reflective boundary condition is applied to minimize artificial reflections, under the assumption that the incoming and outgoing waves are perpendicular to the boundaries (Zijlema et al., 2011):

$$u_b = \pm\sqrt{\frac{g}{h}(2\eta_b - \eta)} \quad (3.2.26)$$

in which u_b is the inflow velocity at the boundary and η_b is the surface elevation signal of the incident wave. Furthermore, a radiation condition based on Sommerfeld's formulation is applied to ensure that outgoing long waves exit the domain smoothly. This condition assumes that outgoing waves propagate with a constant velocity, normal to the boundary. For a boundary parallel to the y-axis, the radiation condition is expressed as:

$$\frac{\partial u}{\partial t} + \sqrt{gh}\frac{\partial u}{\partial x} = 0 \quad (3.2.27)$$

Additionally, a sponge layer boundary condition can be employed to further dissipate wave energy near the edges of the domain effectively. A full description of the numerical model is presented in Zijlema and Stelling (2008) and in Zijlema et al. (2011).

5. References

Albertini, C., Miglino, D., Bove, G., De Falco, M., De Paola, F., Dinuzzi, A. M., … & Manfreda, S. (2022). Integration of a probabilistic and a geomorphic method for the optimization of flood detention basins design. Environmental Sciences Proceedings, 21, 9. https://doi.org/10.3390/environsciproc2022021009

Amore, E., Modica, C., Nearing, M. A., & Santoro, V. C. (2004). Scale effect in USLE and WEPP application for soil erosion computation from three Sicilian basins. Journal of Hydrology, 293(1–4), 100–114. https://doi.org/10.1016/j.jhydrol.2004.01.018

Anita, G., Sandri, L., Marzocchi, W., Argnani, A., Gasparini, P., & Selva, J. (2012). Probabilistic tsunami hazard assessment for Messina Strait Area (Sicily, Italy). Natural Hazards, 64(1), 329–358. https://doi.org/10.1007/s11069-012-0246-x

Arcas, D., & Uslu, B. (2010). A Tsunami Forecast Model for Crescent City, California. NOAA OAR Special Report.

Arnold, J. G., Srinivasan, R., Muttiah, R. S., & Williams, J. R. (1998). Large Area Hydrologic Modeling and Assessment Part 1: model development. JAWRA Journal of the American Water Resources Association, 34(1), 73-89. https://doi.org/10.1111/j.1752-1688.1998.tb05961.x

ASCE (2022). Minimum design loads and associated criteria for structures and other structures.

Auddino, M., Dominici, R., & Viscomi, A. (2015). Evaluation of yield sediment in the Sfalassà Fiumara (southwestern, Calabria) by using Gavrilović method in GIS enviroment. Rendiconti Online Società Geologica Italiana, 33, 3–7. https://doi.org/10.3301/ROL.2015.01

Balistrocchi, M., Grossi, G., & Bacchi, B. (2013). Deriving a practical analytical-probabilistic method to size flood routing reservoirs. Advances in Water Resources, 62, 37–46. https://doi.org/10.1016/j.advwatres.2013.09.018

Basili, R., Brizuela, B., Herrero, A., Iqbal, S., Lorito, S., Maesano, F. E., … & Zaytsev, A. (2021). The Making of the NEAM Tsunami Hazard Model 2018 (NEAMTHM18). Frontiers in Earth Science, 8. https://doi.org/10.3389/feart.2020.616594

Bernard, E. N., Mofjeld, H. O., Titov, V., Synolakis, C. E., González, F. I., Purvis, M. J., … & Robertson, R. E. A. (2006). Tsunami: scientific frontiers, mitigation, forecasting and policy implications. Philosophical Transactions of the Royal Society A: Mathematical, Physical and Engineering Sciences, 364(1845), 1989–2007. https://doi.org/10.1098/rsta.2006.1809

Bernard, E., & Titov, V. (2015). Evolution of tsunami warning systems and products. Philosophical Transactions of the Royal Society A: Mathematical, Physical and Engineering Sciences, 373(2053). https://doi.org/10.1098/rsta.2014.0371

Bertola, M., Viglione, A., Lun, D., Hall, J., & Blöschl, G. (2020). Flood trends in Europe: are changes in small and big floods different? Hydrology and Earth System Sciences, 24(4), 1805-1822. http://dx.doi.org/10.5194/hess-24-1805-2020

Bonaventura, L., Gatti, F., Menafoglio, A., Rossi, D., Brambilla, D., Papini, M., & Longoni, L. (2021). An efficient and robust soil erosion model at the basin scale. MOX-Report, 34, 41.

Brambilla, D., Papini, M., Ivanov, V. I., Bonaventura, L., Abbate, A., & Longoni, L. (2020). Sediment yield in mountain basins, analysis, and management: the SMART-SED project. Applied Geology, 43–59. https://doi.org/10.1007/978-3-030-43953-8_3

Brambilla, D., Papini, M., & Longoni, L. (2018). Temporal and spatial variability of sediment transport in a mountain river: A preliminary investigation of the Caldone river, Italy. Geosciences, 8(5). https://doi.org/10.3390/geosciences8050163

Brune, G. M. (1953). Trap efficiency of reservoirs. Eos, Transactions American Geophysical Union, 34(3), 407–418. https://doi.org/10.1029/TR034i003p00407

Casson Moreno, V., Reniers, G., Salzano, E., & Cozzani, V. (2018). Analysis of physical and cyber security-related events in the chemical and process industry. Process Safety and Environmental Protection, 116, 621–631. https://doi.org/10.1016/j.psep.2018.03.026

Castro Rodriguez, D. J. (2024). Modelling Industrial Vulnerabilities within a multi-hazard framework for the resilience of the territories. PhD thesis, Politecnico di Torino.

Cecioni, C., Iorio, V., Bellotti, G., & Grilli, S. T. (2023). Probabilistic landslide tsunami modeling of the 2018 Palu Bay event. Coastal Engineering, 183. https://doi.org/10.1016/j.coastaleng.2023.104332

CNR (2018). Istruzioni per la valutazione della robustezza delle costruzioni.

Copernicus (2023). Corine Land Cover. https://land.copernicus.eu/

Corti, M., Ghirlanda, E., Mainetti, M., Abbate, A., De Vita, P., Calcaterra, D., … & Longoni, L. (2023). Evaluation of the applicability of sediment transport models to dam filling prediction in different Italian geological contexts. Italian Journal of Engineering Geology and Environment, 27–32. https://doi.org/10.4408/IJEGE.2023-01.S-04

Davoudi, S., Brooks, E., & Mehmood, A. (2013). Evolutionary resilience and strategies for climate adaptation. Planning Practice and Research, 28(3), 307–322. https://doi.org/10.1080/02697459.2013.787695

Day, T. (2006). Degree-days: theory and application. Tm41, 106.

Di Baldassarre, G., Montanari, A., Lins, H., Koutsoyiannis, D., Brandimarte, L., & Bloschl, G. (2010). Flood fatalities in Africa: from diagnosis to mitigation. Geophysical Research Letters, 37(22). https://doi.org/10.1029/2010GL045467

Douglas-Mankin, K. R., Srinivasan, R., & Arnold, J. G. (2010). Soil and water assessment tool (SWAT) model: current developments and applications. Transactions of the ASABE, 53(5), 1423–1431. https://doi.org/10.13031/2013.34915

DPCM (2017). Siam directive n.128, 05/06/2017. https://www.protezionecivile.gov.it/it/normativa/direttiva-pcm-istituzione-siam-0/

Dunbar, P. K., Stroker, K. J., Brocko, V. R., Varner, J. D., McLean, S. J., Taylor, L. A., … & Warnken, R. R. (2008). Long-Term Tsunami Data Archive Supports Tsunami Forecast, Warning, Research, and Mitigation. In: Cummins, P.R., Satake, K., Kong, L.S.L. (eds). Tsunami Science Four Years after the 2004 Indian Ocean Tsunami, 2275–2291. https://doi.org/10.1007/978-3-0346-0057-6_15

Eagleson., P. S. (1972). Dynamics of Flood Frequency. Water Resources Research, 8(4), 878–898. https://doi.org/10.1029/WR008i004p00878

European Commission (2018). Report from the Commission to the European Parliament and the Council - On the implementation of the EU Strategy on adaptation to climate change. COM(2018) 738 Final, 19. https://eur-lex.europa.eu/legal-content/EN/TXT/?uri=COM:2018:738:FIN

European Commission (2021). Report from the Commission to the European Parliament and the Council On the implementation and efficient functioning of Directive 2012/18/EU on the control of major-accident hazards involving dangerous substances for the period 2015-2018. 2021, 1–17.

European Union Parliament (2012). Directive 2012/18/EU on the control of major-accident hazards involving dangerous substances, amending and subsequently repealing Council Directive 96/82/EC, L197 Official Journal of the European Union § (2012). https://eur-lex.europa.eu/legal-content/EN/TXT/?uri=CELEX%3A32012L0018%0Ahttps://eur-lex.europa.eu/eli/dir/2012/18/oj%0Ahttp://eur-lex.europa.eu/LexUriServ/LexUriServ.do?uri=OJ:L:2012:197:0001:0037:EN:PDF

European Union Parliament (2022). Directive (EU) 2022/2557 of the European Parliament and of the Council of 14 December 2022 on the resilience of critical entities and repealing Council Directive 2008/114/EC (2022). Retrieved from http://data.europa.eu/eli/dir/2022/2557/oj

Farr, T. G., Rosen, P. A., Caro, E., Crippen, R., Duren, R., Hensley, S., … & Alsdorf, D. E. (2007). The shuttle radar topography mission. Reviews of Geophysics, 45(2). https://doi.org/10.1029/2005RG000183

FEMA (2012). Guidelines for design of structures for vertical evacuation from tsunamis. (FEMA P-646).

Flanagan, D. C., & Livingston, S. J. (1995). WEPP user summary, (11), 141.

Gatti, F., Bonaventura, L., Menafoglio, A., Papini, M., & Longoni, L. (2023). A fully coupled superficial runoff and soil erosion basin scale model with efficient time stepping. Computers and Geosciences, 177, 105362. https://doi.org/10.1016/j.cageo.2023.105362

Gatti, F., Menafoglio, A., Togni, N., Bonaventura, L., Brambilla, D., Papini, M., & Longoni, L. (2021). A novel downscaling procedure for compositional data in the Aitchison geometry with application to soil texture data. Stochastic Environmental Research and Risk Assessment, 35(6), 1223–1241. https://doi.org/10.1007/s00477-020-01900-2

Gavrilovic, Z. (1988). The use of an empirical method (erosion potential method) for calculating sediment production and transportation in unstudied or torrential streams.

Geist, E. L., & Parsons, T. (2006). Probabilistic analysis of tsunami hazards. Natural Hazards, 37(3), 277–314. https://doi.org/10.1007/s11069-005-4646-z

Gete, Z., Winter, T., & Flanagan, D. (1999). BPCDG: Breakpoint Climate Data Generator for WEPP Using Observed Standard Weather Data Sets, 1–17.

Giandotti, M. (1934). Previsione delle piene e delle magre dei corsi d'acqua. Istituto Poligrafico dello Stato (Vol. 8).

Gioia, A., Iacobellis, V., Manfreda, S., & Fiorentino, M. (2008). Runoff thresholds in derived flood frequency distributions. Hydrology and Earth System Sciences, 12(6), 1295–1307. https://doi.org/10.5194/hess-12-1295-2008

Gioia, A., Iacobellis, V., Manfreda, S., & Fiorentino, M. (2012). Influence of infiltration and soil storage capacity on the skewness of the annual maximum flood peaks in a theoretically derived distribution. Hydrology and Earth System Sciences, 16(3), 937–951. https://doi.org/10.5194/hess-16-937-2012

Glimsdal, S., Løvholt, F., Harbitz, C. B., Romano, F., Lorito, S., Orefice, S., … & Omira, R. (2019). A new approximate method for quantifying tsunami maximum inundation height probability. Pure and Applied Geophysics, 176(7), 3227–3246. https://doi.org/10.1007/s00024-019-02091-w

González, F. I., Geist, E. L., Jaffe, B., Kânoğlu, U., Mofjeld, H., Synolakis, C. E., … & Yalciner, A. (2009). Probabilistic tsunami hazard assessment at Seaside, Oregon, for near-and far-field seismic sources. Journal of Geophysical Research: Oceans, 114(11). https://doi.org/10.1029/2008JC005132

Grezio, A., Babeyko, A., Baptista, M. A., Behrens, J., Costa, A., Davies, G., … & Thio, H. K. (2017). Probabilistic tsunami hazard analysis: multiple sources and global applications. Reviews of Geophysics, 55(4), 1158–1198. https://doi.org/10.1002/2017RG000579

Hargreaves, G. H., & Allen, R. G. (2003). History and Evaluation of Hargreaves Evapotranspiration Equation. Journal of Irrigation and Drainage Engineering, 129(1), 53–63. https://doi.org/10.1061/(asce)0733-9437(2003)129:1(53)

Hiemstra, P. (2013). Automap: automatic interpolation package. R package. https://cran.r-project.org/web/packages/automap/automap.pdf

Hollnagel, P. E., Leveson, P. N., Woods, P. D. D., & Woods, D. (2006). Resilience Engineering: Concepts and Precepts. CRC Press Taylor & Francis Group. Ed., 1st, ed. New York, NY.

Hosseini S, Barker K, & Ramirez-Marquez J E. (2016). A review of definitions and measures of system resilience. Reliability Engineering and System Safety, 145(1), 47–61. https://doi.org/10.1016/j.ress.2015.08.006

Iacobellis, V., & Fiorentino, M. (2000). Derived distribution of floods based on the concept of partial area coverage with a climatic appeal. Water Resources Research, 36(2), 469–482. https://doi.org/10.1029/1999WR900287

Intergovernmental Panel on Climate Change (2023). Climate Change 2021 – The Physical Science Basis: Working Group I Contribution to the Sixth Assessment Report of the Intergovernmental Panel on Climate

Change., 1st ed. Masson-Delmotte, V., P. Zhai, A. Pirani, S.L. Connors, C. Péan, S. Berger, N. Caud, Y. Chen, L. Goldfarb, M.I. Gomis, M. Huang, K. Leitzell, E. Lonnoy, J.B.R. Matthews, T.K. Maycock, T. Waterfield, O. Yelekçi, R. Yu, and B. Zhou, Cambridge University Press, Cambridge, United Kingdom and New York, NY, USA. https://doi.org/10.1017/9781009157896

ISPRA (2023). Inventario Seveso D.Lgs. 105/2015. Inventario degli stabilimenti a rischio di incidenti rilevanti connessi con sostanze pericolose. https://www.rischioindustriale.isprambiente.gov.it/seveso-query-105/Default.php

ISRIC (2021). Soilgrids - global gridded soil information. https://soilgrids.org/

Jain, P., Pasman, H. J., Waldram, S. P., Rogers, W. J., & Mannan, M. S. (2017). Did we learn about risk control since Seveso? Yes, we surely did, but is it enough? An historical brief and problem analysis. Journal of Loss Prevention in the Process Industries, 49, 5–17. https://doi.org/10.1016/j.jlp.2016.09.023

Kaiser, G., Scheele, L., Kortenhaus, A., Løvholt, F., Römer, H., & Leschka, S. (2011). The influence of land cover roughness on the results of high resolution tsunami inundation modeling. Natural Hazards and Earth System Science, 11(9), 2521–2540. https://doi.org/10.5194/nhess-11-2521-2011

Kanamori, H. (1972). Mechanism of tsunami earthquakes. Physics of the Earth and Planetary Interiors, 6(5), 346–359. https://doi.org/10.1016/0031-9201(72)90058-1

Koshimura, S., & Shuto, N. (2015). Response to the 2011 Great East Japan Earthquake and Tsunami disaster. Philosophical Transactions of the Royal Society A: Mathematical, Physical and Engineering Sciences, 373(2053). https://doi.org/10.1098/rsta.2014.0373

Kostadinov, S., Braunović, S., Dragićević, S., Zlatić, M., Dragović, N., & Rakonjac, N. (2018). Effects of erosion control works: Case study - Grdelica Gorge, the South Morava River (Serbia). Water, 10(8), 1094. https://doi.org/10.3390/w10081094

Kottegoda, N. T., & Rosso, R. (2008). Applied Statistics for Civil and Environmental Engineers. Wiley-Blackwell.

Labonté-Raymond, P. L., Pabst, T., Bussière, B., & Bresson, É. (2020). Impact of climate change on extreme rainfall events and surface water management at mine waste storage facilities. Journal of Hydrology, 590. https://doi.org/10.1016/j.jhydrol.2020.125383

Lay, T., Kanamori, H., Ammon, C. J., Nettles, M., Ward, S. N., Aster, R. C., … & Sipkin, S. (2005). The great Sumatra-Andaman earthquake of 26 December 2004. Science, 308(5725), 1127–1133. https://doi.org/10.1126/science.1112250

Lin, I.-C., & Tung, C. C. (1982). A preliminary investigation of tsunami hazard. Bulletin of the Seismological Society of America, 72(6A), 2323–2337. https://doi.org/10.1785/bssa07206a2323

Lorito, S., Selva, J., Basili, R., Romano, F., Tiberti, M. M., & Piatanesi, A. (2015). Probabilistic hazard for seismically induced tsunamis: accuracy and feasibility of inundation maps. Geophysical Journal International, 200(1), 574–588. https://doi.org/10.1093/gji/ggu408

Løvholt, F., Griffin, J., & Salgado-Gálvez, M. A. (2022). Tsunami Hazard and Risk Assessment on the Global Scale. Complexity in Tsunamis, Volcanoes, and Their Hazards, 213–246. https://doi.org/10.1007/978-1-0716-1705-2_642

Lynett, P., Weiss, R., Renteria, W., De La Torre Morales, G., Son, S., Arcos, M. E. M., & MacInnes, B. T. (2013). Coastal Impacts of the March 11th Tohoku, Japan Tsunami in the Galapagos Islands. Pure and Applied Geophysics, 170(6–8), 1189–1206. https://doi.org/10.1007/s00024-012-0568-3

Madsen, P. A., Fuhrman, D. R., & Schäffer, H. A. (2008). On the solitary wave paradigm for tsunamis. Journal of Geophysical Research: Oceans, 113(12). https://doi.org/10.1029/2008JC004932

Madsen, P. A., & Schäffer, H. A. (2010). Analytical solutions for tsunami runup on a plane beach: single waves, N-waves and transient waves. Journal of Fluid Mechanics, 645, 27–57. https://doi.org/10.1017/S0022112009992485

Manfreda, S., & Fiorentino, M. (2008). A stochastic approach for the description of the water balance dynamics in a river basin. Hydrology and Earth System Sciences, 12(5), 1189–1200. https://doi.org/10.5194/hess-12-1189-2008

Manfreda, S., Miglino, D., & Albertini, C. (2021). Impact of detention dams on the probability distribution of floods. Hydrology and Earth System Sciences, 25(7), 4231–4242. https://doi.org/10.5194/hess-25-4231-2021

Maris, F., Vasileiou, A., Tsiamantas, P., & Angelidis, P. (2019). Estimating the future function of the Nipsa reservoir due to climate change and debris sediment factors. Climate, 7(6), 76. https://doi.org/10.3390/cli7060076

Masud, S., & Khan, A. (2024). Policy implementation barriers in climate change adaptation: the case of Pakistan. Environmental Policy and Governance, 34(1), 42–52. https://doi.org/10.1002/eet.2054

Mazzoglio, P., Butera, I., & Claps, P. (2020). I^2-RED: a massive update and quality control of the Italian annual extreme rainfall dataset. Water, 12(12). https://doi.org/10.3390/w12123308

Merz, B., Blöschl, G., Vorogushyn, S., Dottori, F., Aerts, J. C. J. H., Bates, P., … & Macdonald, E. (2021). Causes, impacts and patterns of disastrous river floods. Nature Reviews Earth and Environment, 2(9), 592–609. https://doi.org/10.1038/s43017-021-00195-3

Minister for Civil Protection and Sea Policies (2022). Directive of December 7, 2022 - Part 1-"Guidelines for the preparation of the external emergency plan," Part 2-"Guidelines for information to the population," and Part 3-"Guidelines for the testing of external emergency plans"- pursuant to Article 21, Paragraph 7 of Legislative Decree No. 105 of June 26, 2015, "Implementation of Directive 2012/18/EU on the control of major-accident hazards involving dangerous substances." Italian Official Gazette No. 31, February 7, 2023.

Ministry of Public Works Decree (2001). Minimum safety requirements in urban and territorial planning for areas affected by establishments at risk of major accidents. Italian Official Gazette No. 138 16/06/-Ordinary Supplement No. 151Official Journal of Italian Republic.

Mori, N., Takahashi, T., Yasuda, T., & Yanagisawa, H. (2011). Survey of 2011 Tohoku earthquake tsunami inundation and run-up. Geophysical Research Letters, 38(18). https://doi.org/10.1029/2011GL049210

Mulvaney, T.J. (1851). On the use of self-registering rain and flood gauges in making observations of the relations of rainfall and flood discharges in a given catchment. Proceedings of the Institution of Civil Engineers of Ireland, 4, 19–31. http://ci.nii.ac.jp/naid/10025316839/en/

NatCatSERVICE. (2010). Munich Re NatCatSERVICE. www.munichre.com/en/reinsurance/business/non life/georisks/natcatservice/default.aspx

Neitsch, S. L., Arnold, J. G., Kiniry, J. R., Williams, J. R., & KKing, K. W. (2002). Soil and Water Assessment Tool (SWAT) User's Manual, Version 2000, Grassland Soil and Water Research Laboratory. Texas Water Resources Institute, College Station, 13(04), 52–55.

NERC (1975). Estimation of flood volumes over different durations. Flood Studies Report Vol. 1, 243–264.

Nicks, A., Lane, L., & Gander, G. (1995). Chapter 2: Weather generator. In USDA Water Erosion Prediction Project: Hillslope Profile and Watershed Model Documentation. D. C. Flanagan and M.A. Nearing, eds. NSERL Report No 10 (p. 22).

NTC (2018). Norme tecniche per le costruzioni - aggiornamento delle norme tecniche per le costruzioni. www.gazzettaufficiale.it/eli/id/2018/2/20/18A00716/

Oishi, Y., Imamura, F., & Sugawara, D. (2015). Near-field tsunami inundation forecast using the parallel TUNAMI-N2 model: Application to the 2011 Tohoku-Oki earthquake combined with source inversions. Geophysical Research Letters, 42(4), 1083–1091. https://doi.org/10.1002/2014GL062577

Pilgrim, D. H., & McDermott, G. E. (1981). Design floods for small rural catchments in Eastern New South Wales. National Conference Publication - Institution of Engineers, Australia, (81 /7), 138–142.

Pilone, E., Casson Moreno, V., Cozzani, V., & Demichela, M. (2021). Climate change and NaTech events: a step towards local-scale awareness and preparedness. Safety Science, 139. https://doi.org/10.1016/j.ssci.2021.105264

Pilone, E., Demichela, M., & Camuncoli, G. (2017). Seveso Directives and LUP: the mutual influence of natural and anthropic impacts. Journal of Loss Prevention in the Process Industries, 49, 94–102. https://doi.org/10.1016/j.jlp.2017.02.027

Presidenza del Consiglio dei Ministri - Dipartimento della Protezione Civile (2018). Indicazioni alle componenti ed alle strutture operative del servizio nazionale di protezione civile per l'aggiornamento delle pianificazioni di protezione. https://www.gazzettaufficiale.it/gazzetta/serie generale/caricaDettaglio? dataPubblicazioneGazzetta=2018-11-15&numeroGazzetta=266.

Rallison, R. E. (1980). Origin and Evolution of the Scs Runoff Equation, 912–924.

Regione Lombardia (2021). ARPA Lombardia. https://www.arpalombardia.it/

Regione Lombardia (2023). Geoportale della Regione Lombardia. https://www.geoportale.regione.lombardia.it/

Rickenmann, D. (1994). Alternative equation for the mean velocity in gravel-bed rivers and mountain torrents. Proceedings - National Conference on Hydraulic Engineering, (pt 1), 672–676.

Rickenmann, D. (2001). Comparison of bed load transport in torrents and gravel bed streams. Water Resources Research, 37(12), 3295–3305. https://doi.org/10.1029/2001WR000319

Röbke, B. R., & Vött, A. (2017). The tsunami phenomenon. Progress in Oceanography, 159, 296–322. https://doi.org/10.1016/j.pocean.2017.09.003

Rodriguez-Iturbe, I., Porporato, A., Ridolfi, L., Isham, V., & Cox, D. R. (1999). Probabilistic modelling of water balance at a point: the role of climate, soil and vegetation. Proceedings of the Royal Society A: Mathematical, Physical and Engineering Sciences, 455(1990), 3789–3805. https://doi.org/10.1098/rspa.1999.0477

Rossi, F., & Villani, P. (1994). Valutazione delle Piene in Campania. Salerno.

Shakou, L. M., Wybo, J. L., Reniers, G., & Boustras, G. (2019). Developing an innovative framework for enhancing the resilience of critical infrastructure to climate change. Safety Science, 118, 364–378. https://doi.org/10.1016/j.ssci.2019.05.019

Sørensen, M. B., Spada, M., Babeyko, A., Wiemer, S., & Grünthal, G. (2012). Probabilistic tsunami hazard in the Mediterranean Sea. Journal of Geophysical Research: Solid Earth, 117(1). https://doi.org/10.1029/2010JB008169

Srinivasan, R., J.G. Arnold, T.S. Ramanarayanan, & S. T. B. (2000). Modeling Wister lake watershed with the soil and water assessment tool (SWAT). Journal American Water Resources Association.

Synolakis, C. E., & Bernard, E. N. (2006). Tsunami science before and beyond Boxing Day 2004. Philosophical Transactions of the Royal Society A: Mathematical, Physical and Engineering Sciences, 364(1845), 2231–2265. https://doi.org/10.1098/rsta.2006.1824

Synolakis, C., & Kânoğlu, U. (2015). The Fukushima accident was preventable. Philosophical Transactions of the Royal Society A: Mathematical, Physical and Engineering Sciences, 373(2053). https://doi.org/10.1098/rsta.2014.0379

Tadepalli, S., & Synolakis, C. E. (1996). Model for the leading waves of tsunamis. Physical Review Letters, 77(10), 2141–2144. https://doi.org/10.1103/PhysRevLett.77.2141

Tanioka, Y., & Satake, K. (1996). Tsunami generation by horizontal displacement of ocean bottom. Geophysical Research Letters, 23(8), 861–864. https://doi.org/10.1029/96GL00736

Tarquini, S., Isola, I., Favalli, M., & Battistini, A. (2007). TINITALY, a digital elevation model of Italy with a 10 meters cell size.

Titov, V. V., & Synolakis, C. E. (1997). Extreme inundation flows during the Hokkaido-Nansei-Oki tsunami. Geophysical Research Letters, 24(11), 1315–1318. https://doi.org/10.1029/97GL01128

Titov, V., Rabinovich, A. B., Mofjeld, H. O., Thomson, R. E., & Gonzàlez, F. I. (2005). The global reach of the 26 December 2004 Sumatra tsunami. Science, 309(5743), 2045–2048. https://doi.org/10.1126/science.1114576

Tonini, R., Di Manna, P., Lorito, S., Selva, J., Volpe, M., Romano, F., … & Vittori, E. (2021). Testing tsunami inundation maps for evacuation planning in Italy. Frontiers in Earth Science, 9. https://doi.org/10.3389/feart.2021.628061

Veloso Lima, V., Avilez-Valente, P., Viana Baptista, M. A., & Miranda, J. M. (2019). Generation of N-waves in laboratory. Coastal Engineering, 148, 1–18. https://doi.org/10.1016/j.coastaleng.2019.02.012

Volpi, E., Di Lazzaro, M., Bertola, M., Viglione, A., & Fiori, A. (2018). Reservoir effects on flood peak discharge at the catchment scale. Water Resources Research, 54(11), 9623–9636. https://doi.org/10.1029/2018WR023866

Yuan, Y., Li, H., Wei, Y., Shi, F., Wang, Z., Hou, J., … Xu, Z. (2021). Probabilistic tsunami hazard Assessment (PTHA) for Southeast coast of Chinese mainland and Taiwan Island. Journal of Geophysical Research: Solid Earth, 126(2). https://doi.org/10.1029/2020JB020344

Zhang, G., Liu, Y., Han, Y., & Zhang, X. C. (2009). Sediment Transport and Soil Detachment on Steep Slopes: I. Transport Capacity Estimation. Soil Science Society of America Journal, 73(4), 1291–1297. https://doi.org/10.2136/sssaj2008.0145

Zijlema, M., & Stelling, G. S. (2008). Efficient computation of surf zone waves using the nonlinear shallow water equations with non-hydrostatic pressure. Coastal Engineering, 55(10), 780–790. https://doi.org/10.1016/j.coastaleng.2008.02.020

Zijlema, M., Stelling, G., & Smit, P. (2011). SWASH: an operational public domain code for simulating wave fields and rapidly varied flows in coastal waters. Coastal Engineering, 58(10), 992–1012. https://doi.org/10.1016/j.coastaleng.2011.05.015